ABSTRACT

Title of Thesis:	INVESTIGATION OF SCRAMJET PERFORMANCE DURING COMBUSTION MODE TRANSITION
	Marvellous M. Achugbu,
	Master of Science, 2025
Thesis Directed By:	Professor Kenneth H. Yu, Department of Aerospace Engineering

Combustion mode transition is a key challenge in dual-mode ramjet engines (DMRJ) due to its direct effect on the engine's performance and operation. DMRJs are designed to operate both in a ramjet mode at lower supersonic speeds and in a scramjet mode at higher speeds. The investigation of the engine's performance during the combustion mode transition is desirable to ensure continuous engine operability over the transitional Mach numbers. Depending on the flight speeds, the combustion mode can switch from subsonic combustion mode, commonly known as thermally choked mode, to supersonic combustion mode and vice versa. This study investigates and quantifies the effects of these transitions on combustor stability and propulsion performance metrics.

The mode transition is expected to occur near the start of the hypersonic flight regime. Combustion mode transition experiments were conducted using a laboratory-scale, direct-

connect test facility that employed a vitiated air heater to match the enthalpy of Mach 5 flight conditions at an altitude of 19 km. A convergent-divergent supersonic nozzle was used to establish a Mach 2 isolator entrance flow which defined the upstream boundary conditions. The combustor model featured one fuel injector upstream of the cavity flame-holder and three more fuel injectors downstream. Previous studies have shown that natural mode transition occurs at or near the critical equivalence ratio in a series of sporadic transitions back and forth over a relatively substantial length of time spanning around 400~600 msec. This study investigates and quantifies the effects of these transitions on combustor stability and propulsion performance metrics.

High-frequency dynamic pressure measurements and axial distribution of wall pressure were measured at various equivalence ratios near the mode transition conditions. The results showed that combustion instabilities are observed during the natural mode transition process at or near the critical equivalence ratio of 0.24. The dominant oscillations were observed at 957 ± 10 Hz with a peak amplitude of 0.2 psi. Also, a cycle analysis was performed to investigate the effect of mode transition on instantaneous thrust. Using previously obtained velocity data and wall pressure measurements, local thrust function was computed, and the cycle analysis was extended into an assumed pressure-matched exit nozzle. The cycle analysis results revealed a substantial effect of combustion mode transition on expected thrust level, changing the amplitude by more than 13%. Finally, a mode transition control strategy is discussed that can not only avoid the combustion instability but also reduce the sudden disruption caused by thrust change associated with the mode transition.

INVESTIGATION OF SCRAMJET PERFORMANCE DURING COMBUSTION MODE TRANSITION

by

Marvellous M. Achugbu

Thesis submitted to the Faculty of the Graduate School of
The University of Maryland College Park, in partial fulfillment
of the requirements for the degree of
Master of Science
2025

Advisory Committee:
Professor Dr. Kenneth H. Yu, Chair/Advisor
Professor Dr. Raymond J. Sedwick
Professor Dr. Sung W. Lee

Dedication

This work is dedicated to my lovely parents, my brother, my sisters, my nieces, my friends, and a special someone for the continuous love, encouragement, and support they showed me throughout this journey. I will forever be grateful to my now-late dad for indulging me in the ways of engineering, pushing me further than he was able to go, and giving me more than enough courage to make me achieve the things he could not without forcing or imposing his dreams on me, as we both shared similar dreams and aspirations in life. Thank you for always being there for me and raising me to be the type of man I am today. For the surplus wisdom you imparted to me, I would always say you were one of the three wise men who came from the East. I will carry your legacy, and I miss our nerdy talks. Thank you, Mom, for taking care of me and ensuring I eat even when locked up in my room studying. I truly appreciate you and Dad's sacrifices for me and my siblings. You both are the *best parents* I could have ever asked for.

Thank you, TD boys, for keeping me on my toes to keep up with you guys. I still believe we are the best set of TD boys BFS will ever have. Thank you, Sodiq, Ganiyu, Kester, Enny, and Marvellous (girl), for being amazing. Lastly, to my special someone, thank you, Yin!

Acknowledgments

Most importantly, I would like to thank my advisor, Dr. Kenneth H. Yu, for being such an amazing professor, mentor, and person. I thank you for your time, effort, and commitment to helping me write my success story and making me a better engineer. He is always readily available and able to modify his already complex schedule to attend to my needs.

I want to thank members of my committee for taking the time to read and review this thesis. Thank you for your guidance and constructive criticism, as they have made me a better person and helped me think critically about the matters brought to my attention. I would like to extend my gratitude to Dr. Raymond Sedwick for standing by me during hard times and supporting me in achieving my goals. I appreciate Dr. Sung Lee for honing my leadership skills, making me trust my instincts, and developing my intuition. Also, I would like to acknowledge and thank the Science, Mathematics, and Research for Transformation (SMART) program and my sponsor facility, Naval Air Systems Command (NAVAIR), for funding my graduate education and research at the university.

Lastly, I would like to thank the present Advanced Propulsion Research Laboratory team Ramakrishnan C, Alan Tchamourliyski, Andrew Szabo, and Rahulreddy Pinninti for their contributions in supporting the experiment and prioritizing my research. Special thanks to Ramakrishnan C for his guidance and mentorship throughout the experiments, Alan Tchamourliyski for helping in data analysis and helping understand the experiments, and Mithuun Kanapathipillai for making himself readily available to explain some processes and misunderstood procedures.

Table of Contents

List of Tables

List of Figures

List of Abbreviations

2	Downstream of Shock or Isolator Inlet / Isolator Inlet
3	Combustor Inlet
Φ	Combustor Equivalence Ratio
e	Nozzle Exit Conditions used for Thermodynamic Analysis
M	Mach Number
P_0	Stagnation Pressure / Total Pressure
P	Static Pressure
T_0	Stagnation Temperature / Total Temperature
T	Static Temperature
U	Flow Velocity
γ	Specific Heat Ratio
∞	Freestream or Flight Condition depending on Experiment
H	Isolator Height (0.0127 m = 0.5 in.)
t	Time
Tss	Steady state time
x	Axial Coordinat

Chapter 1: Introduction

1.1 Background and Motivation

There are many reasons for an interest in hypersonic travel among humans, including the ability to cover long distances in a small amount of time, technological advancement, and military dominance. The hypersonic regime begins at Mach 5, that is, at five times the speed of sound. It could drastically cut the travel time across a vast distance, perhaps allowing passengers to travel between continents within a few hours. For example, a hypersonic passenger vehicle can fly from New York to London in under two hours [1]. Research on hypersonic travel started about in the middle of the 20th century [2]. Most of this was fueled by Dr. Wernher von Braun's research in rocketry and aerospace technology during and after WW2. Of these earliest major hypersonic initiatives, the X-15 program, which was started in the 1950s, was named to the highest extent [3]. This rocket plane, developed by NASA and the United States Air Force, could reach speeds of up to Mach 6.7 and altitudes of 100 km. This program produced much-needed data for hypersonic flight and helped inform the design of future space vehicles. One other historical impact on hypersonics came in the Cold War Era in the 1960s, when the United States and the Soviet Union both allocated significant resources to hypersonics both for military use and for the space race [4]. This competition resulted in many experimental aircraft and missile programs to investigate hypersonic flight and its use. The propulsive interest in traveling in a hypersonic flow regime has developed in recent decades in response to advances in material science, computational fluid dynamics (CFD), and propulsion technologies. Recent military programs include five U.S. DARPA projects flown by the Falcon Project, Russia's Avangard

hypersonic glide vehicle, and China's DF-ZF hypersonic glide vehicle, designed for next-generation hypersonic weapons and delivery systems. On the commercial side, Boeing, Lockheed Martin, and Hermeus have all ventured into hypersonic technologies. The need for space tourism and possible intercontinental travel continues to drive research and development.

1.2 Innovations in Supersonic Combustion Ramjet (SCRAMJET)

The scramjet concept evolved from earlier energy conversion work, with the ramjet engine invented in 1913 and its application for propulsion first proposed by the French engineer René Lor in that same year when he recognized that ram pressure could be used in a propulsion device. Thereby eliminating the compressor required for a conventional jet engine.

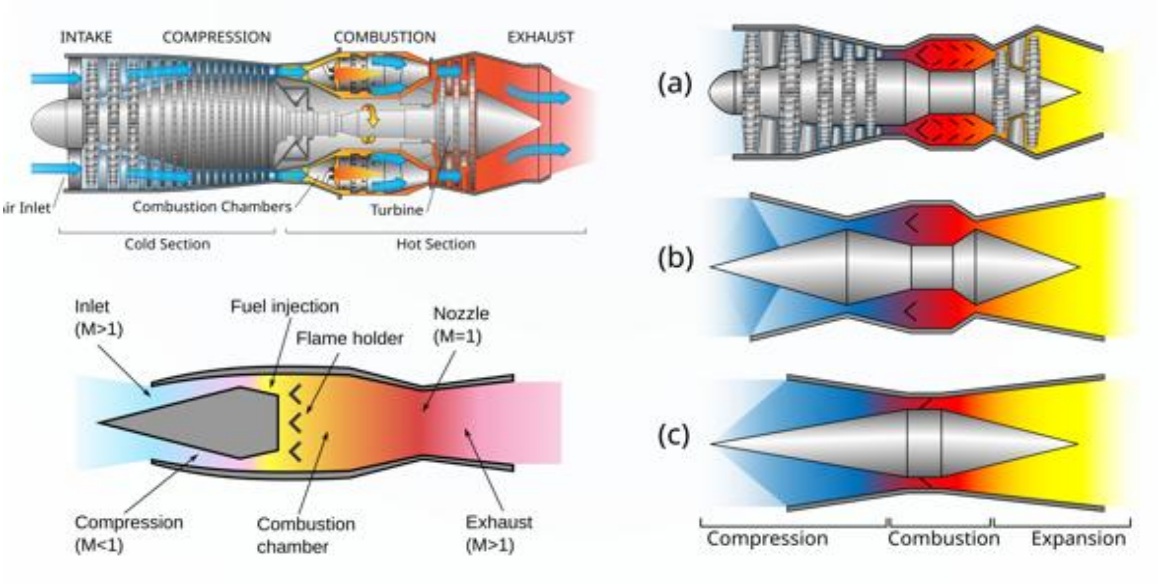

Figure 1.1: Innovation of jet engine from Turbojet to Scramjet (comparative diagram of turbojet, ramjet, and scramjet engines) [5, 6]

Figures b and c show that the blue lines correspond to the shock wave that occurs within the engine. This causes the pressure to increase quite a bit while air is sucked into the inlet at high speeds. If a compressor were used in this situation, it would cause drag and starve the engine's airflow. Instead of the compressor, the ramjet uses a unique area ratio to pressurize the airflow, which has resulted in a diffuser-style shape in the inlet portion. Much of the shape of the diffuser itself is to generate the necessary shockwaves to generate that compression of the incoming high-speed air. This also reduces flow area, which is needed to control airflow dynamics. The shock waves generated are powerful enough not only to reduce the Mach number to subsonic speed. Thus, facilitating combustion in a ramjet engine (left figure below) and also in a scramjet engine (also in Figure 1.2 to the right). The scramjet engine's diffuser (right of Figure 1.2) is a constant area diffuser (also known as the isolator). The first one is the isolator, which enables the scramjet engine to operate between the thermally choked mode and the scramjet mode [9] One more handy function of the isolator is that it serves as the preventer against inlet unstart. It achieves this through containment and blocking the train of shocks from transmitting upstream of the engine inlet. Every hypersonic vehicle creates a shockwave due, largely, to the geometry of the engine, compressing air through a reduction in area. Unlike conventional scramjet engines, the scramjet engine does not use a diffuser but rather balances the flow dynamics established by its shape. To determine the minimal extent required to bring the inlet air to a combustion-ready velocity in the isolator portion, the Fanno flow analysis would be employed.

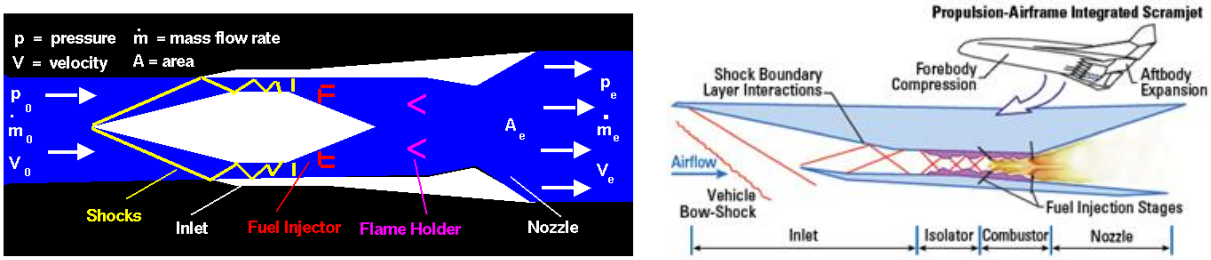

Figure 1.2: Ramjet and Scramjet engines showing the formation of shock [7, 8]

1.3 Combustor

Dual-mode Scramjet engines operate in two different combustion modes. In the first mode, the velocity of the air going to the combustion chamber is subsonic, and the temperature is increased due to combustion until the velocity reaches sonic conditions. Hence, restricting the mass flow rate. This is known as thermal choking. A 1-D steady flow analysis called Rayleigh flow is usually conducted to explain this process, as shown in Figure 1.3. In the second mode of operation, the velocity of the air at the inlet of the combustion chamber is still supersonic. Thus, requiring more fuel for mixing is necessary for efficient combustion. This mode of operation is known as the supersonic combustion mode.

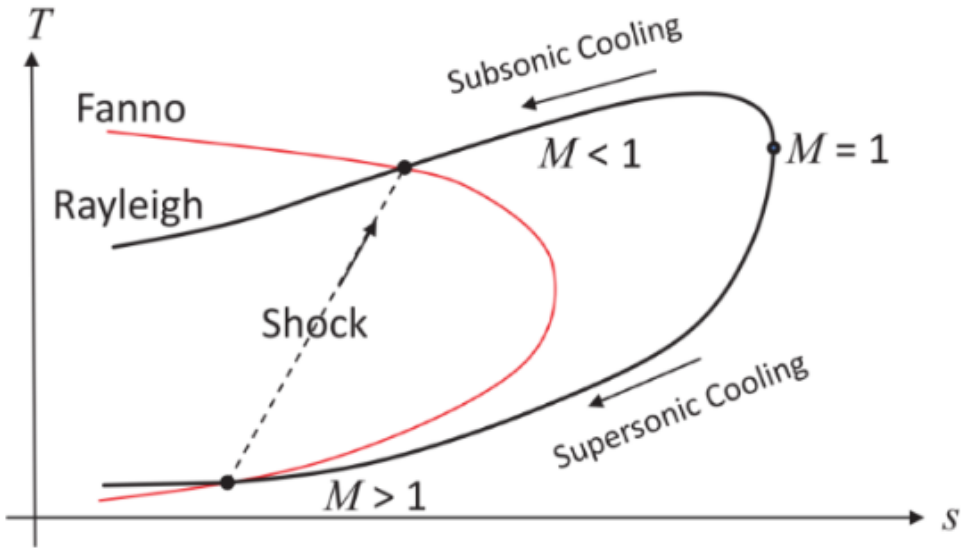

Figure 1.3: Rayleigh and Fanno flow line, adapted from Stephan [10]

The maximum thrust produced from a ramjet engine occurs when the temperature in the combustor is thermally choked (when the temperature is at its maximum). This requires the proper fuel-to-air ratio and proper mixing to achieve this. In Rayleigh flow, the properties vary with the addition of heat. The entropy, velocity, and stagnation temperature increase, and the density, dynamic pressure, and stagnation pressure decrease when Mach is subsonic. The temperature and enthalpy depend on the relationship between the Mach number and the gas constant. When Mach is supersonic, only stagnation pressure and velocity decrease. These can be summarized in Table 1.1.

Table 1.1: Summary of Property Variations with Heating

	M<1	M>1
s	increase	increase
T_0	increase	increase
P_0	decrease	decrease
u or M	increase	decrease
P	decrease	increase
ρ	decrease	increase
T or h	increase if M < $1/\sqrt{\gamma}$ decrease if M > $1/\sqrt{\gamma}$	increase

1.4 Challenges in Scramjet

As the speed of incoming air increases, achieving efficient combustion becomes more challenging. This is because it is difficult to maintain the flame long enough to maximize enthalpy per unit volume and produce maximum thrust. This issue arises from flame quenching, where the flame is extinguished before complete combustion can occur. To address this, engineers have developed flame holders, also known as cavities, to prevent flame quenching. Figure 1.4 shows a cavity in the combustion chamber of a scramjet configuration engine.

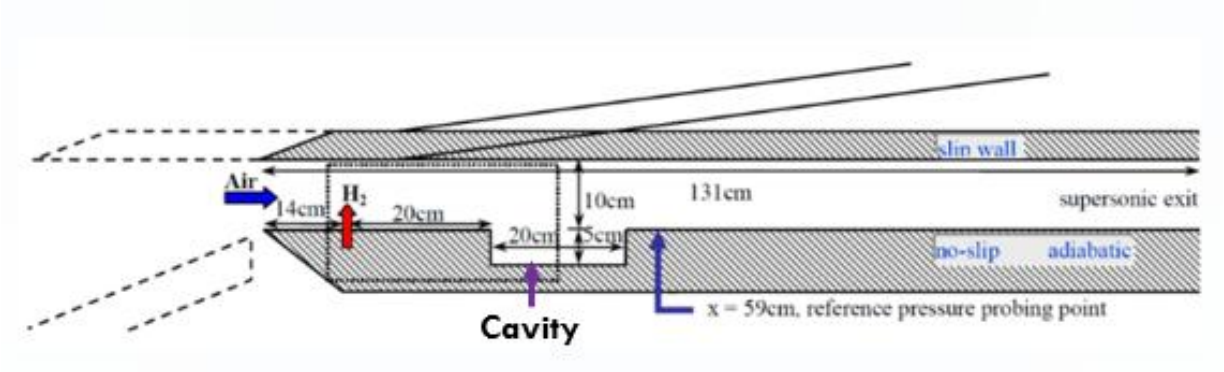

Figure 1.4: Configuration of a scramjet engine showing a Cavity, adapted from [11]

Numerous studies have been conducted to tackle the challenges associated with scramjet engines. These studies focus on ensuring proper mixing of the incoming air with fuel and precisely controlling the amount of fuel injected to avoid waste and achieve complete atomization. Active control of combustion modes significantly enhances overall engine combustion stability [12]. Additionally, research has shown that when mode transition occurs naturally, it often results in frequent mode hopping. In contrast, active control experiments demonstrate a stable one-way transition. This topic will be discussed in greater detail in Chapter 2.

1.4.1 Atmospheric Air Composition

The atmosphere's composition switches fast with height, with an example presented in Figure 1.5 for the NASA NRLMSIS Atmospheric Model. The atmospheric pressure at lower altitudes is dominated by nitrogen molecules (N_2) and oxygen molecules (O_2), which make up about 99% of the total atmosphere. At greater heights, however, atmospheric pressure decreases and molecular diffusion takes over, reducing these gases' relative concentrations. The

dominance of lighter atoms such as atomic oxygen (O), helium (He), and hydrogen (H) above 100 km also suggests the transition from the mesosphere, at altitudes where gases are well-mixed, to the thermosphere, where there is a beginning to be a stratification based on molecular mass, where atomic oxygen becomes the most abundant gas at altitudes around 200–600 km due to the photodissociation of O_2 by ultraviolet solar radiation, and helium and hydrogen dominate at altitudes greater than 600 km because of their relatively low molecular weights and weak gravitational binding. However, within the airbreathing flight corridor the composition of air does not change. Thus, O_2 still remains at 21% by mole.

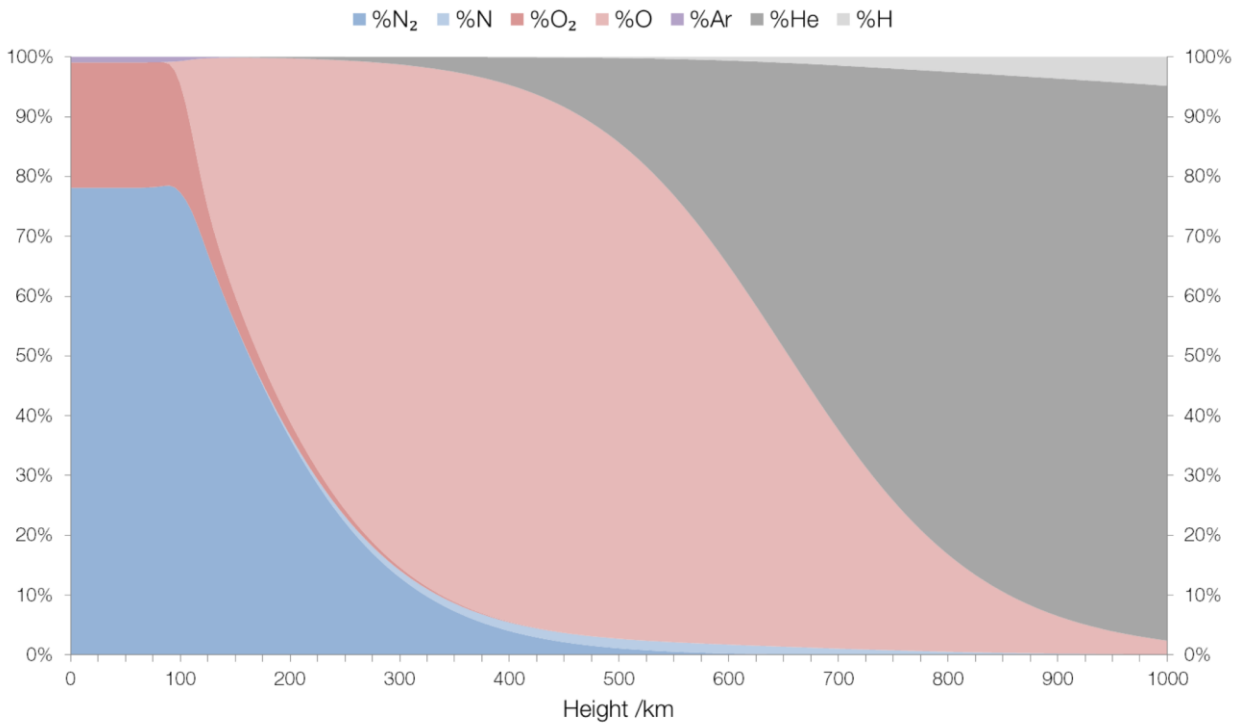

Figure 1.5: NASA NRLMSIS Atmospheric Model [31]

These variations have significant implications for atmospheric dynamical processes, satellite drag, space weather, etc. In addition, its waning density and changing makeup with altitude influence thermal conduction, chemical reactions, and ionospheric qualities that are vital to satellite communications and navigation systems. For example, atomic oxygen is very abundant at high altitudes and thus is quite aggressive against satellite materials. Studies such as Picone et al. [32] enhanced models like NRLMSISE-00, simplifying atmospheric density and composition prediction for such models, whereas Emmert et al. [33] have expanded on them to describe long-term trends in thermosphere composition given their potential impact on climate and space weather. Thus, atmospheric modeling is critical to all scientific and technical undertakings, and the factors highlighted above help articulate the need and demand for accurate modeling.

1.4.2 Engine Operational Limit

Figure 1.6 illustrates the operational regime of air-breathing propulsion systems and their associated flight limitations in terms of altitude versus Mach number. The left [form] is the engine types listed by their effective altitudes and Mach numbers: piston engines (P) at relatively low (1) altitudes (0 to 30000 ft), turboprop engines (TP) at a low effective altitude but at a higher Mach number range (0 to 0.78), turbofan engines (TF) with an effective altitude of 0 to 95000 and a 0 to 0.9 Mach range; turbojet engines (TJ) are found at a slightly higher effective altitude (0 to 40000 ft) than TF and a slightly lower Mach number; and ramjet/scramjet engines (RJ) with the highest effective altitudes. Piston engines and turboprops are optimized for low altitude and subsonic speeds, losing utility as air density drops as altitude increases. The density of the air is much lower at high altitudes and transonic to supersonic speeds, enabling turbojets and turbofans to compress and efficiently employ the thinner air. Ramjets and scramjets do not

have rotating components like a compressor and work best at high supersonic to hypersonic speeds and at altitudes over 60,000 feet, compressing incoming air simply from forward motion.

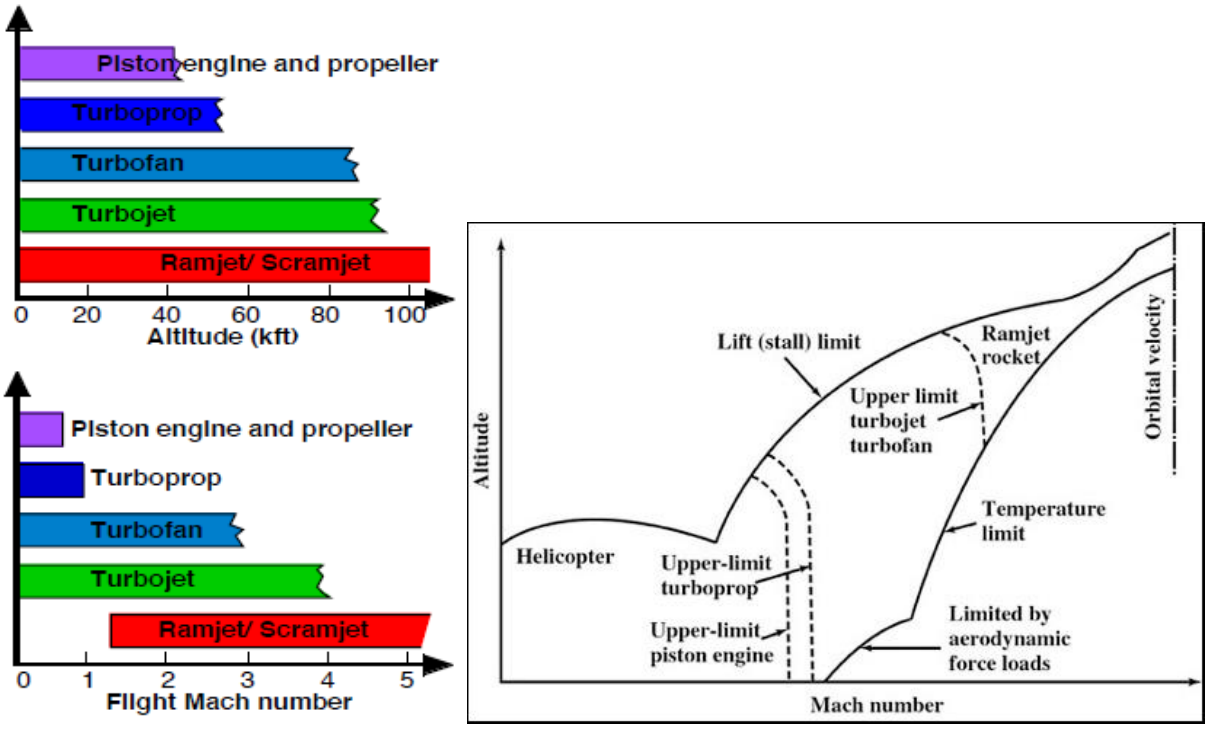

Figure 1.6: Flight Limits of Air-Breathing Engines [34]

The right diagram shows the wider thermal bounds for air-breathing engines when practical limitations are also considered. Aerodynamic and mechanical limitations restrict both helicopters and piston engines to lower altitudes and subsonic speeds. Turboprops and turbofans lead to higher altitudes and supersonic regimes, but their performance is limited by temperature and material limits. Turbojets morph into the upper Mach regime but are superseded by ramjets/scramjets at hypersonic speeds where air compression from forward motion is

important. However, aerodynamic force loads, thermal limitations, and eventual stall regimes determine the upper limits of these engine operating envelopes.

1.4.3 Earth's Atmosphere

Atmospheric properties are crucial to the design, analysis, and operation of aerospace vehicles, which can span subsonic aircraft, hypersonic vehicles, and space reentry systems. Or, the change of atmospheric parameters like T, P, and ρ with altitude affect the aerodynamic forces, propulsion efficiency, as well as structural design. It is also key that we learn the relationships between Mach number, altitude, and dynamic pressure so that we can design flight paths optimally and ensure that our vehicles remain within operational boundaries at all times. Figure 1.7 gives a vertical profile of the Earth's atmosphere and how its temperature and pressure leak as a function of altitude. The layers of the atmosphere (troposphere, stratosphere, mesosphere, and thermosphere) are characterized and distinguished by their thermal gradients. For example, in the troposphere, temperature decreases with altitude; in the stratosphere, temperature neutralizes due to heating from ozone; and in the mesosphere and thermosphere, temperature varies. Pressure (on a logarithmic scale) reduces exponentially as we go to altitude, removing the atmospheric density. These measures are important for realizing the atmospheric drag and thermal behavior of space vehicles in various altitude ranges [35]. The second image in Figure 1.7 shows the runaway drop in pressure and density with altitude and the relatively minuscule decrease in gravity from the radius of the Earth. These variations are important for calculating aerodynamic loads and fuel needs. Panel three shows the dynamic pressure (q) as a function of altitude and Mach number. Dynamic pressure is an important parameter in hypersonic flight because it governs aerodynamic heating and structural loads. The curves show that the lower

density of the air at higher altitudes requires higher Mach numbers to yield the same dynamic pressures. Knowledge of the aerodynamic behavior of vehicles at high speeds is fundamental for the design of flight envelopes and vehicle structures within these regimes [37].

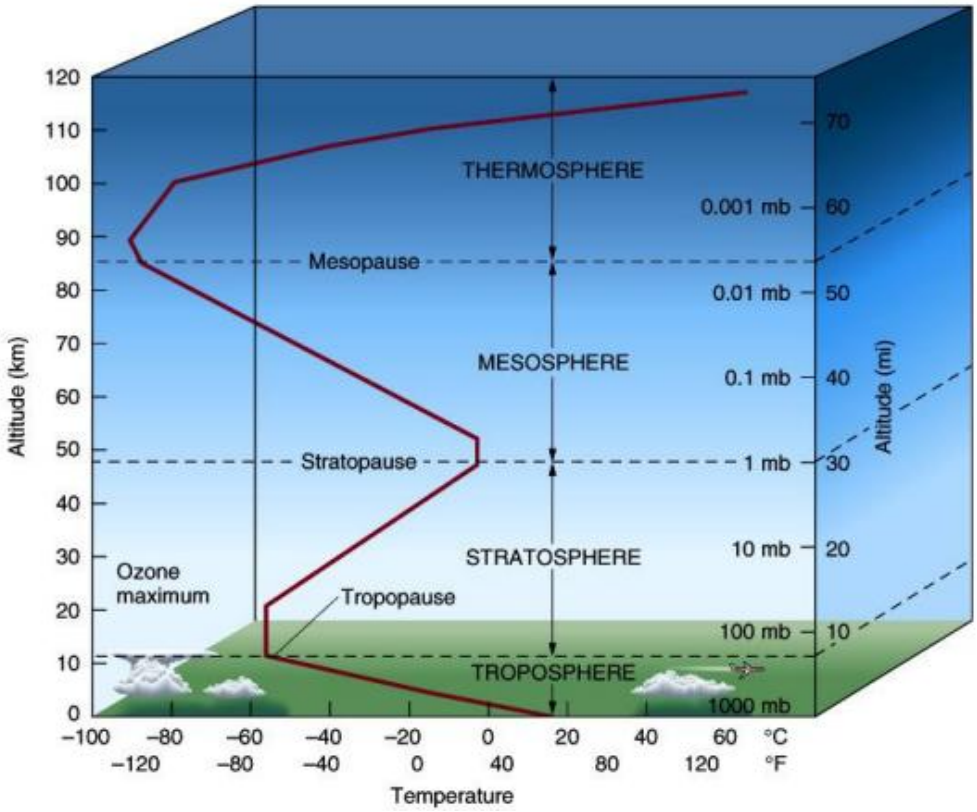

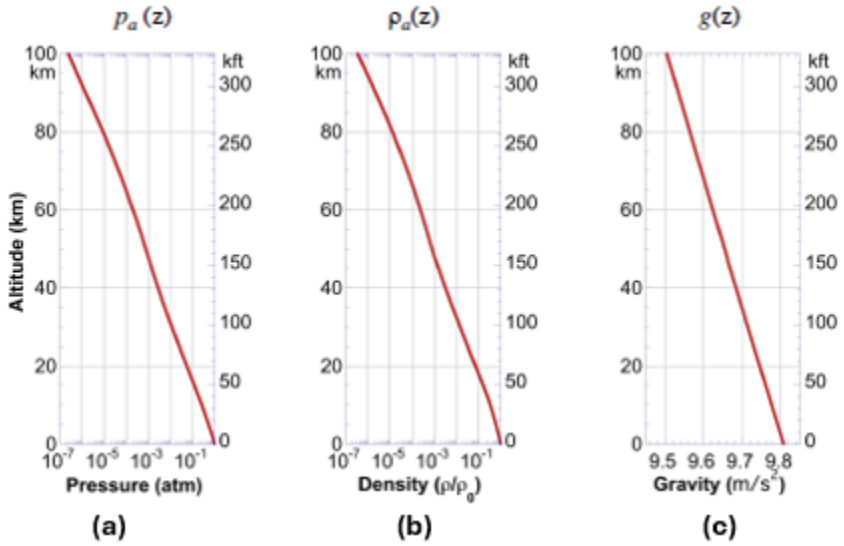

Figure 1.7: Altitude, Pressure, and Temperature as well as Pressure, Density, and Gravity. vs. Altitude [36]

1.5 Technical Objective

This research investigates the performance of scramjets during the transition between the combustion modes. That is, to see the effect the transition between thermally choked mode and supersonic combustion mode would have on the scramjet engine performance, such as thrust. The motivation behind this work emerges from the combustion dynamics and stability of a scramjet engine, as well as understanding the behavior of the engine during the combustion transition modes still being studied. Previous studies have investigated the wall pressure in the combustion chamber of a dual-mode scramjet, especially during the peak operation of the two combustion modes. For this reason, this work investigates how the transition between the combustion modes affects the scramjet engine performance. To be exact, the technical objectives include:

1. To investigate the effect of a dual-mode scramjet combustion mode transition on its performance both experimentally and analytically using a model with an enthalpy-matched vitiated air facility.
    (a) Specifically confirming natural mode transition occurs, and analyze the effects of the combustion mode transition on thrust using experimental data and quantifying the change in uninstalled thrust through thermodynamic cycle analysis.
2. To compare the wall pressure measurements along the axial flow field with the dynamic pressure measurements of the combustor during natural transition mode.

3. Establish an operational strategy to minimize the effect of the transition between the scramjet combustion modes on the performance of the scramjet engine.

Chapter 2: Combustion Mode Shift and Stability

2.1 Combustion Mode Transition

This is common in ramjet engines transitioning into scramjets when the engine reaches higher speeds. With increasing velocity, the airflow through the engine becomes supersonic, and if the engine is to operate efficiently at high speeds, the notion of supersonic combustion must be introduced [14, 15, 16]. The dual-mode scramjet engine can operate in ramjet mode or switch to scramjet mode. This ability is critical for providing performance over a broad spectrum of speeds. Define-rays, a technical term for the Rayleigh flow analysis wherein the transition back to ramjet mode, or thermal choking, occurs via the paradox that heat is released. This process includes a great increase in pressure and temperature, which can strangle the airflow, making the engine return to subsonic combustion [12, 16]. The fuel-air equivalence ratio has been shown in experiments to have a major influence on the thermal choking behavior of scramjet engines. Tuning this ratio changes the combustion characteristics, which affects how well the engine transitions between the modes. The results show how critical it is to control how much fuel is injected as well as how well it mixes, as these factors affect performance [13, 16]. More recently, researchers have investigated the effects of different inlet Mach numbers and fuel-air equivalence ratios on the nature and extent of interaction during mode transitions. The method, once tested in subsonic combustion for scramjet engines, is leading to significant progress in understanding the location of ignition and the formation of various unwanted combustion phenomena [12, 13, 16]. Figure 2.1 highlights important features of scramjet engines and scramjet engine operation to aid comprehension.

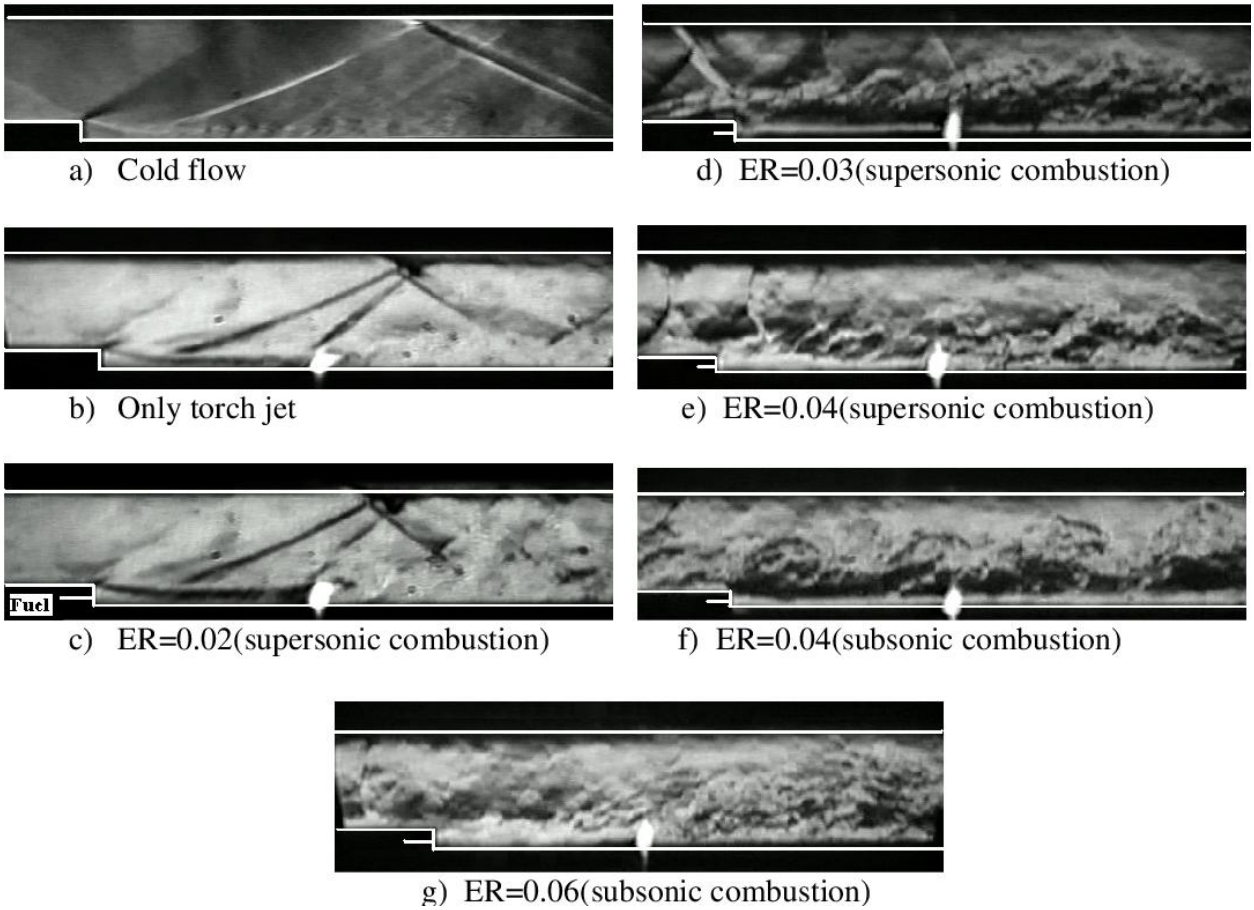

Figure 2.1: An illustration of a scramjet engine configuration operating in ramjet mode and scramjet mode, adapted from [17]

Scramjet engines undergo a two-stage combustion transition process that is influenced by various factors such as speed, pressure, temperature, and equivalence ratio. These transitions are important for the efficient performance of scramjet engines for sustained hypersonic applications. These transition types and associated experiments are being continually researched as the field advances towards practical implementations, such as hypersonic propulsion development. In order to understand the transition between the modes, we need to be able to

understand the challenges in stabilizing the combustion of scramjet engines and the modes of operation of the combustor individually.

2.2 Fuel injection and mixing

Efficient combustion in scramjets depends heavily on how well the fuel is mixed with the incoming supersonic air stream. Scramjet engines, which operate at hypersonic speeds, face significant challenges related to fuel injection and mixing. This is because, at these high speeds, the time available for fuel and air to mix and combust is extremely short, often just a few milliseconds. This poses unique challenges for achieving efficient and stable combustion.

Some of the major problems addressed by researchers in proper fuel mixing include short residence time, fuel atomization, shockwaves formed due to flow dynamics, combustion stability, and injector design. Curran and Murthy showed how short residence time affects effective combustion. Given that the flow velocity is supersonic throughout the engine, this limits the time available for fuel injection, mixing, and combustion. Thus, the residence time t_r can be approximated as shown in Equation 2.1. As speed increases, U becomes large. Thereby, reducing t_r significantly.

$$t_r = \frac{L}{U} \tag{2.1}$$

Another challenge is that the supersonic speed of the airflow creates pressure gradients within the combustion chamber. The presence of this factor can disrupt the fuel spray and hinder effective mixing. Therefore, careful injector design is needed to ensure that the fuel is properly atomized and distributed within the short residence time [18]. Zhao showed how proper atomization of the fuel is critical to ensuring it can mix quickly and thoroughly with the air. Poor

atomization can result in large fuel droplets that are difficult to ignite and burn completely within the limited time available. Equation 2.2 shows the Sauter mean diameter (SMD), a measure of droplet size that should be minimized for efficient combustion. Smaller SMD values indicate better atomization, which enhances mixing and combustion efficiency [21].

$$SMD = \frac{\sum_i n_i d_i^3}{\sum_i n_i d_i^2} \tag{2.2}$$

Also, shockwaves can enhance mixing by creating turbulence and vortices, but they must be carefully controlled to avoid excessive pressure losses. The Mach number M and shock angles are crucial parameters in designing the combustion chamber, as shown in Equation 2.3. The interaction of oblique shocks and expansion fans can be manipulated to enhance mixing while minimizing pressure losses [9].

$$M = \frac{U}{a} \tag{2.3}$$

Some of the solutions found by researchers include maintaining a consistent fuel-to-air ratio by using a steady equivalence ratio, designing effective injectors, numerical simulations, and active control. Combustion requires maintaining a consistent fuel-air mixture. The equivalence ratio ϕ, defined in Equation 2.4, affects combustion stability and efficiency. Variations in ϕ can lead to instabilities such as localized quenching or blowout [18].

$$\phi = \frac{\dot{m}_{O_2 stochiometry}}{\dot{m}_{O_2 actual}} \tag{2.4}$$

Optimizing mixing efficiency requires the effective design of the injectors. To promote this, strut-based and cavity-based injectors are the possible strategies for improving turbulence and rapid mixing [20]. Apply innovative injector designs, like angled and transverse injectors, to add turbulence and mixing zones. This design increases combustion efficiency through a

homogeneous distribution of fuel [12,13, 21]. Injection and mixing processes are simulated and optimized in a scramjet, offering great flexibility, and are commonly defined using computational fluid dynamics (CFD) simulations. This aids investigators in modeling flow interactions that might be too complicated to directly measure and optimize designs [21].

Explorations into mix-enhancing methods such as pulsed fuel injection and plasma-assisted combustion have also been conducted. These approaches adapt the flow field on the fly and improve mixing in real time [9]. Mithuun discussed various cases where stable modes of operation become established. They have to do with changing the way the fuel gets injected. But here we will deal with cases 3(a) & 3(b), which concern the switching between thermally prankled mode, as well as supersonic mode, & we'll go over the respective modes in the sections to come. However, Cases 3(a) and 3(b) are related to the transition between alternative fuel injection schemes while keeping the equivalence ratio fixed. As the overlap obtained from the sequencing is conservative, which is equal to 0.1 s, for case 3(a), overlap occurs during the transition of flow from single injection to distributed injection, and for case 3(b), overlap occurs during the transition from distributed injection to single injection [12]. Figure 2.2 depicts such a pressure rise at x/H = 1, where valve sequencing occurs and the fuel distribution scheme switches from one scheme to the other.

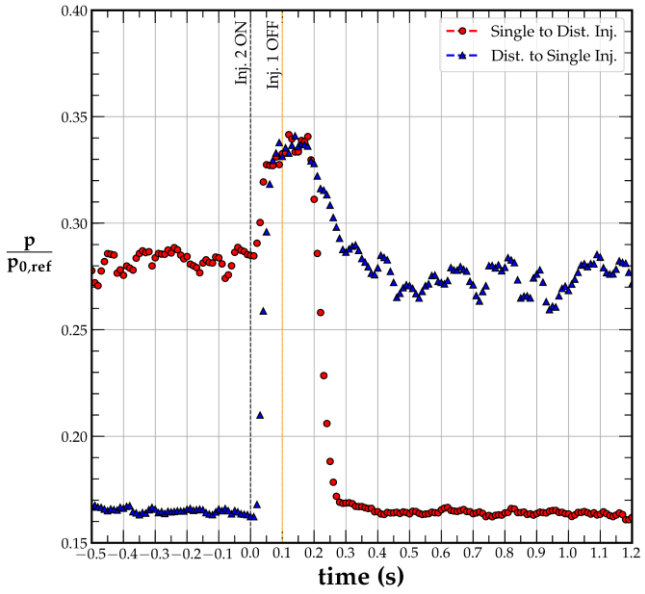

Figure 2.2: Wall pressure vs. time during active control sequencing in the combustor [12].

In both cases, 3(a) and 3(b), Mithuun took the wall pressure at the transition mode. To the left of Figure 2.3 is the pressure-time trace for case 3(a) and the transition from stable, thermally choked mode operation to stable, supersonic combustion operation. To the right of Figure 2.3 is Case 3(b), which depicts the transition from stable supersonic combustion mode to stable thermally choked mode operation. The static wall pressure data shows this transition to occur on the order of 0.3 s for both cases, but luminescence data captured at 10,000 Hz for Case 3(b), as seen in Figure 2.4, shows this transition to be much shorter on the order of 1 msec. Figure 2.3 also shows that the flame rapidly blows off during the transition before re-establishing itself in its new mode. As the active control mechanism switches from one injection scheme to the other, any residual air in the fuel line will cause the flame to blow off and cause the local equivalence ratio to rise downstream [12].

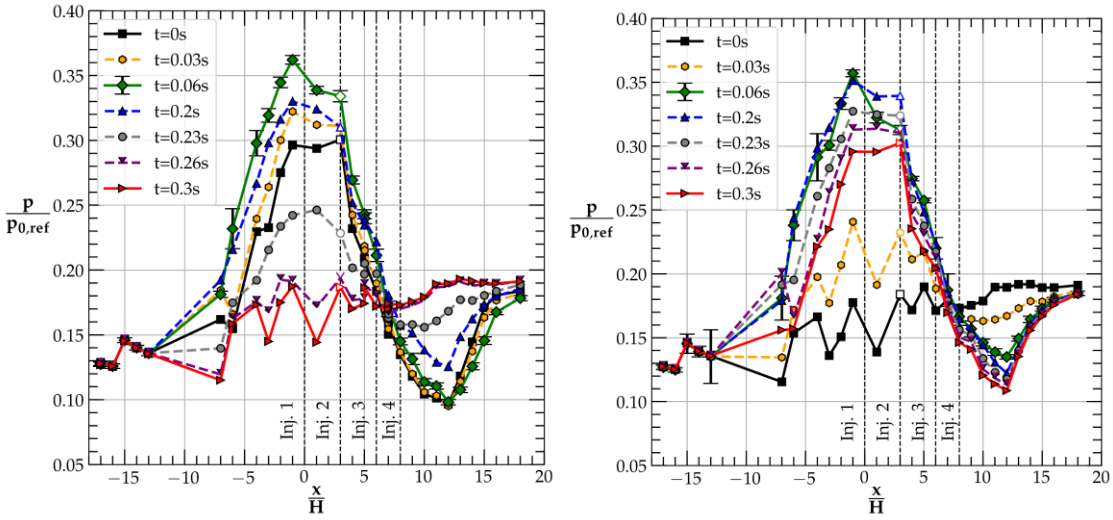

Figure 2.3: Temporal progression of wall pressure trace during actively controlled mode transition of Case 3(a) (single to distributed) (left). Temporal progression of wall pressure trace during actively controlled mode transition of Case 3(b) (distributed to single) (right).

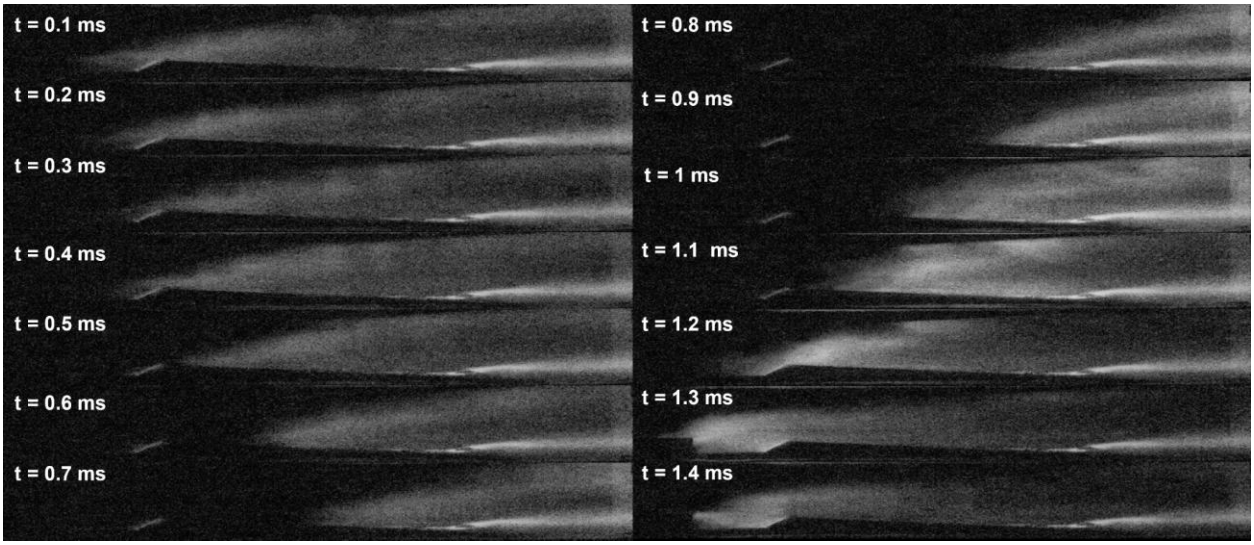

Figure 2.4: Series of high-speed luminescence images at different time intervals depicting the rapid mode transition event from supersonic combustion mode to thermally-choked Mode [12].

2.3 Thermally Choked Combustion Mode

Thermally choked combustion mode in scramjet conditions can be observed when the heat released from combustion is so high that the flow itself is choked, which can be explained using the Rayleigh flow analysis as described before. Now that flow is thermally choked, which means there is a sonic point in the flow path. As a result, we expect this effect to play a central role in the transition between different combustion modes in dual-mode scramjet engines, like the engine used in our study. The phenomenon is mainly driven by the four factors: heat release, mass addition, friction, and flow blockage. In this case, the flow is thermally choked, and a normal shock system is established to reduce the flow to subsonic values downstream. On the other side, scramjet has a scramjet engine isolator as shown in Figure 2.5 of the respective subsonic speeds ahead of the combustion chamber so that combustion could become a proper and stable process. Essentially, the combustion remains stable with the thermal choking effect eliminating the need for a nozzle on a traditional ramjet.

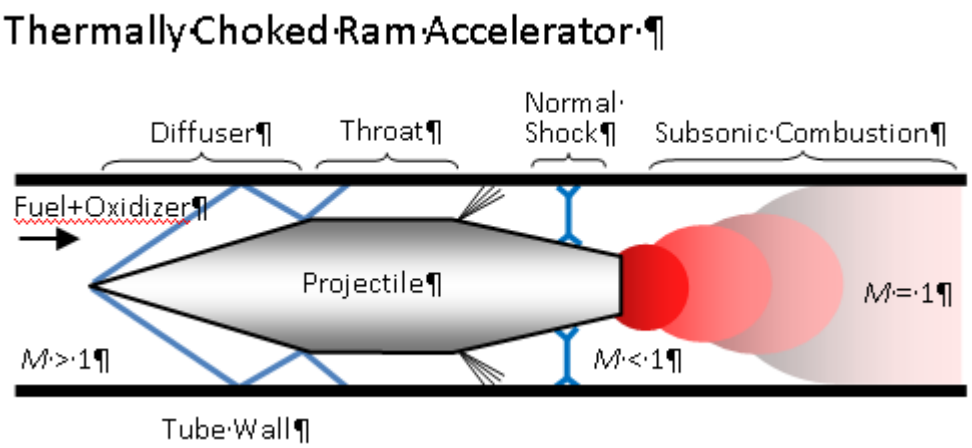

Figure 2.5: Formation of normal shock at the end of the isolator to reduce the flow to subsonic for a thermally choked combustor [22].

Thermal choking is crucial to understanding and controlling scramjets for the efficient design and operation of these engine types. The isolated shock train, which consists of a set of reflexive oblique/normal shocks, acts as a compression source and distributes the resulting pressure rise produced during the downstream reaction [19]. The shock train structure and the flow confinement are mainly controlled by the inflow Mach number.

2.4 Supersonic Combustion Mode

In supersonic combustion mode, the airflow through the engine stays supersonic from the start to the finish of the process, including the combustion chamber (see Figure 2.6). This is in stark contrast to conventional ramjets, in which air flows were decelerated to subsonic velocities ahead of combustion. Scramjets, on the other hand, can run on supersonic combustion and are typically used at much higher velocities, traditionally above Mach 5. It takes a great deal of air to make these scramjets work. They need to be brought up to supersonic speeds typically

by a booster rocket or other propulsion system before the scramjet can be lit. This prime phase of acceleration is vital as scramjets are unable to translate into efficient thrust at lower velocities.

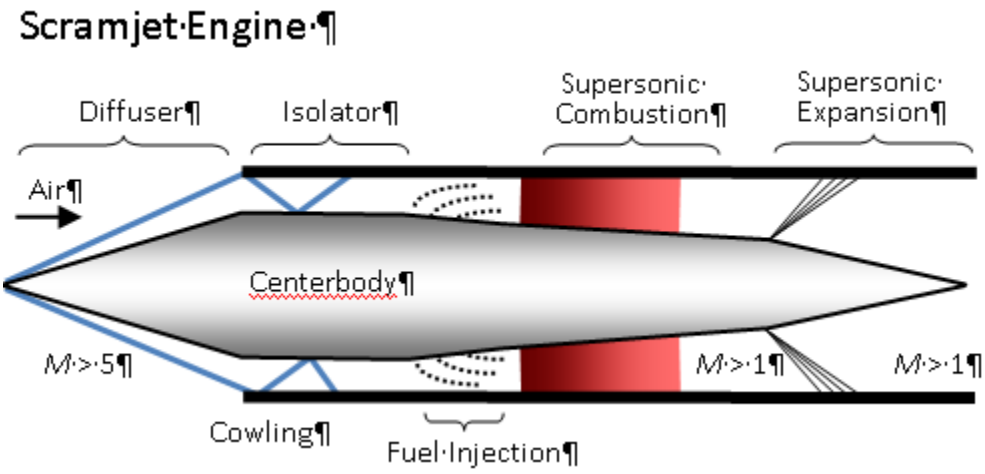

Figure 2.6: Flow is still supersonic in the combustion chamber [22].

2.5 Summary

The transition to the scramjet engine occurs when the speed of the ramjet approaches the supersonic range. These flow velocities make the airflow in the engine supersonic, which requires transitioning the combustion to supersonic to keep the engine functioning properly. A dual-mode scramjet engine is capable of operating in either ramjet or scramjet modes, which is key for maintaining performance through speed ranges. The engine naturally does thermal choking, returning to ramjet mode inside with a significant increase in pressure and temperature, which can also reduce the airflow. How thermal choking works can be drastically improved by altering the fuel ratio to air in the engine. As a result, the fuel injection and mixing must be closely controlled. Hence, effective combustion in scramjet engines greatly depends on the degree of fuel mixing with the supersonic air. The fast speeds at which scramjets work allow

only milliseconds for the fuel to blend with and burn with the air, making it difficult to realize efficient combustion. After being on this “combustion mode” transition in a scramjet engine, withstand the pressure of Mithun’s walls experienced in the experiments discussed. In the first case, the engine transitioned from a stable, thermally choked state to stable supersonic combustion. In the other case, it returned from supersonic combustion to a thermally choked operation. The pressure data suggested that these transitions occurred over roughly 0.3 seconds, but more detailed imaging found that in the second case, the transition occurred much more quickly within just 1 millisecond. The flame in the engine briefly blew out before re-establishing itself in the new mode during that transition. In thermally choked combustion, the heat of combustion itself is so extreme that it 'chokes' the flow and gets the process down to subsonic speeds, which is crucial in specific modes within the operation of an engine. In contrast, supersonic combustion mode maintains supersonic airflow throughout, enabling the engine to remain operational at supersonic speeds, generally above Mach 5 or more. This mode is critical for scramjets, which must first be accelerated to supersonic speeds before they can properly operate.

Chapter 3: Experimental Framework and Diagnostics

Numerous reacting flow experiments were conducted to investigate the effect of the transition from thermally choked mode to supersonic mode and vice versa on performance metrics such as the engine thrust produced, pressure distribution in the combustion chamber, and overall engine stability using a dual-mode scramjet engine combustor model. This chapter highlights the experimental framework and the diagnostic techniques used for this study.

3.1 Direct-Connect Vitiated Heater Facility

George Box states, “All models are wrong, but some are useful.” Hence, to get a realistic or useful result from a model, making sure some conditions, like the flight condition, stay the same is important. To do this, a direct-connect vitiated heater was used to simulate the flight conditions for the experiment. This required the enthalpy of the flight conditions to be matched by raising the temperature of the vitiated air. In conjunction, an Atlas Copco GA 75 Type compressor is used to send high-pressure air to the facility alongside a Hankison HPRP 400-460 dryer used to remove moisture from the incoming airflow. Figure 3.1 shows a schematic diagram of the vitiated heater facility. This builds off the work of Mithuun and Aguilera [12, 13]. After the moisture is removed from the airflow, it enters the facility through a 10.058 mm (0.396 in) metering orifice. Then it goes through an expansion joint, which is used to relieve the structural stress expected by loading due to temperature. A blow-out port is used as a safety medium to prevent any sort of blowback event that might occur, and an expansion coupler is utilized to raise the flow path from a 52.5 mm (2.067 in) to a 77.9 mm (3.068 in) diameter circular section.

The vitiated heater works with the same principle as a gas turbine engine combustor. There is a fuel delivery pipe connected to the gas mixer via a liner cone to generate a fine fuel and air mix to be ignited, as shown in Figure 3.2. A C_2H_4/O_2 igniter is placed downstream of the liner cone, which uses an Auto lite Copper Core Spark Plug. To contain the hydrogen flame and mix the combustion properly with the oxygen injected upstream, a long section with three separate pipes was used. Near the heater exit, 304 stainless steel is used as a straightener prior to the scramjet connection, which was achieved with a customized circular-to-square transition nozzle as shown in Figure 3.3. With a Setra 206 transducer and a K-type thermocouple, stagnation pressure and stagnation temperature measurements were collected. The facility's gaseous fuel and air are delivered by gas bottles and a gas line system. The trials used eight gas lines. The facility's heater uses one fuel line for hydrogen and two gas lines for oxygen and replenishing for the vitiation process. The scramjet uses two gas lines to deliver its main fuel. The remaining three lines feed gaseous oxygen, ethylene, and nitrogen to igniters in the scramjet and heater. Gas tanks include 1/4-turn valves that may be manually shut off in case of an emergency. The valves were originally opened for each test, but gas flow only occurred when a Parker 24V DC solenoid valve was actuated outside. One-way valves were employed to prevent oxidant gas from moving upstream in a fuel supply line. Figure 3.4 depicts the size of the isolator and scramjet combustor. The cavity size is based on earlier studies [13, 23]. The igniter orifice is 1.5H from the cavity's dump plane. The combustor has 6 degrees of expansion, starting at the cavity dump plane.

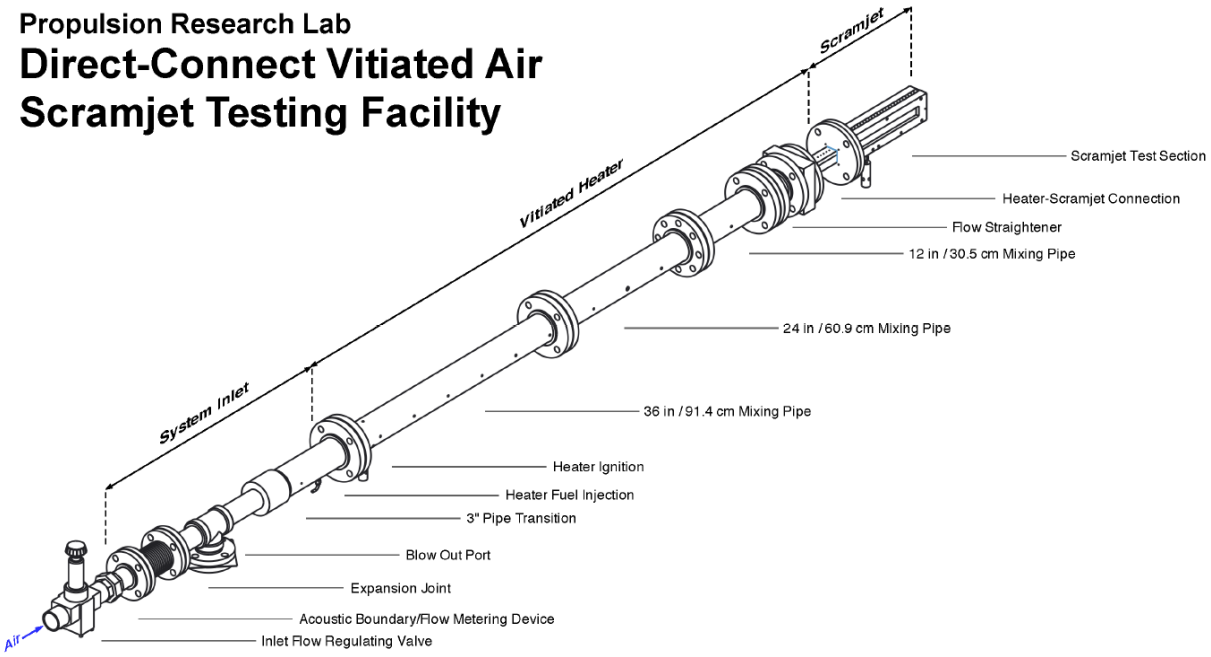

Figure 3.1: Schematic of a direct-connect vitiated heater facility adapted from [12, 13] showing the main components.

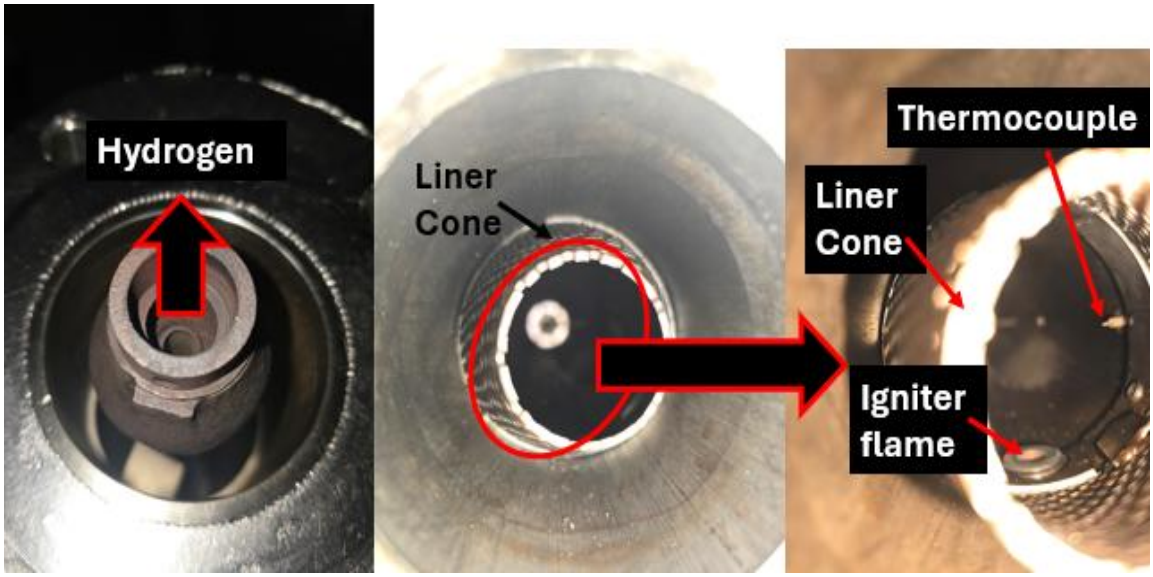

Figure 3.2: Liner cone inside the vitiated heater facility.

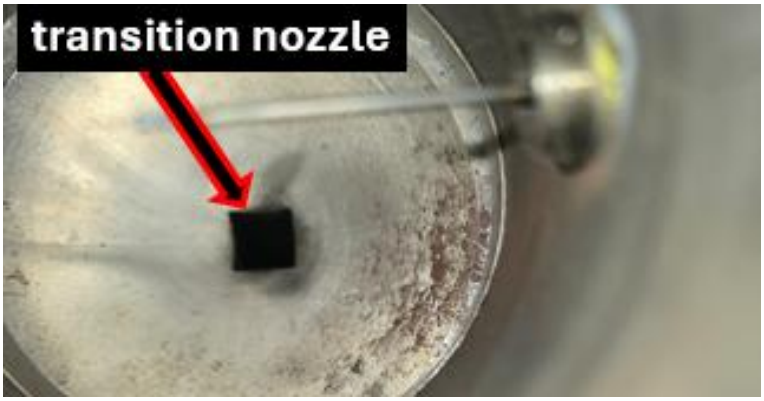

Figure 3.3: Circular to Square Nozzle

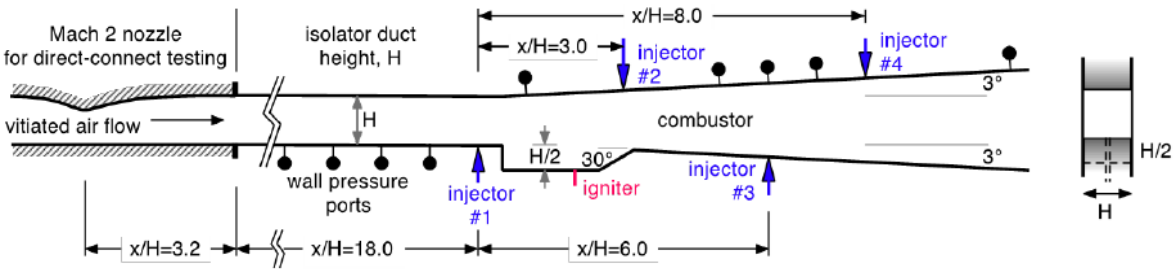

Figure 3.4: Dual-mode scramjet schematic and dimensions [12].

3.2 Test Conditions

George Box states, “All models are wrong, but some are useful.” Hence, to get a realistic or useful result from a model, making sure some conditions, like the flight condition, stay the same is important. Table 3.1 shows the conditions of the vitiated heater obtained using NASA CEA.

Table 3.1: Vitiated Heater (V.H) Conditions

Free Stream Parameters	Symbols	Values
V.H Flow Rate (g/s)	$\dot{m}_{\infty}$	**51.06 ± 0.03**
Free Stream Temperature (K)	$T_{o\infty}$	**1341 ± 20**
Stagnation Pressure (Kpa)	P_o	**502 ± 20**
O_2 Replenishment (g/s)	$\dot{m}_{O_2}$	**17.682 ± 0.01**
H_2 Flow rate (g/s)	$\dot{m}_{H_2}$	**1.439 ± 0.01**
C_2H_4 flow rate (g/s)	$\dot{m}_{C_2H_4}$	**0.905 ± 0.01**
V.H Gas Constant (J/Kg.K)	**R**	**309.7 ± 1.7**
Steady State Time (secs)	T_{SS}	**5-6**
Mach Number	M_3	**2.01 ± 0.05**

Table 3.2 presents the primary cases in which scramjet tests were conducted using gaseous hydrogen as the chosen fuel. In all cases, an ethylene/oxygen mixture igniter was employed to ensure reliable ignition and flame-holding, with data collected after the igniter was turned off. The first two cases operated entirely in the supersonic combustion regime, with equivalence ratios (Φ) of 0.13 and 0.23. The following five cases (Φ = 0.24, 0.25, 0.26, 0.28, and 0.30) were examined due to observed instability, with Φ = 0.24 suspected to mark the transition point. The final two cases corresponded to fully thermally choked combustion, both with Φ of 0.31 and 0.43.

Table 3.2: Scramjet test experimental runs

Case	Combustion Mode	Φ
Case 1a	**Supersonic**	**0.13 ± 0.01**
Case 1b	**Supersonic**	**0.23 ± 0.003**
Case 2a	**Transition**	**0.24 ± 0.003**
Case 2b	**Thermally choked (unstable)**	**0.25 ± 0.003**
Case 2c	**Thermally choked (unstable)**	**0.26 ± 0.003**
Case 2d	**Thermally choked (unstable)**	**0.28 ± 0.003**
Case 2e	**Thermally choked (unstable)**	**0.30 ± 0.003**
Case 3a	**Thermally choked**	**0.31 ± 0.01**
Case 3b	**Thermally choked**	**0.43 ± 0.01**

3.3 Test Sequencing

The quarter-turn valves are opened during a routine test run while NI CompactRIO-9022 activates solenoids for fuel/oxidizer injection. Figure 3.5.1 shows pressure changes in all gas lines of interest with time during a vitiated heater-only test. Test runs are usually 7 seconds long. At t=0, the igniter spark turns on. At t = 1 s, gaseous ethylene and oxygen are injected and ignited in the vitiated heater igniter. The igniter runs for 2 s, turning off at t = 3 s. The primary hydrogen fuel and oxygen for the vitiated heater replenishment begin at t = 2 s and continue until the end of the test at t = 7 s.

In Scramjet combustion tests, as illustrated in Figure 3.5.1, 3.5.2, and 3.5.3, fuel injection is turned on from t = 3 s to t = 7 s from the injector, while the scramjet igniter is on from t = 2.5 s to t = 4 s and fuel is stopped at t = 7 s.

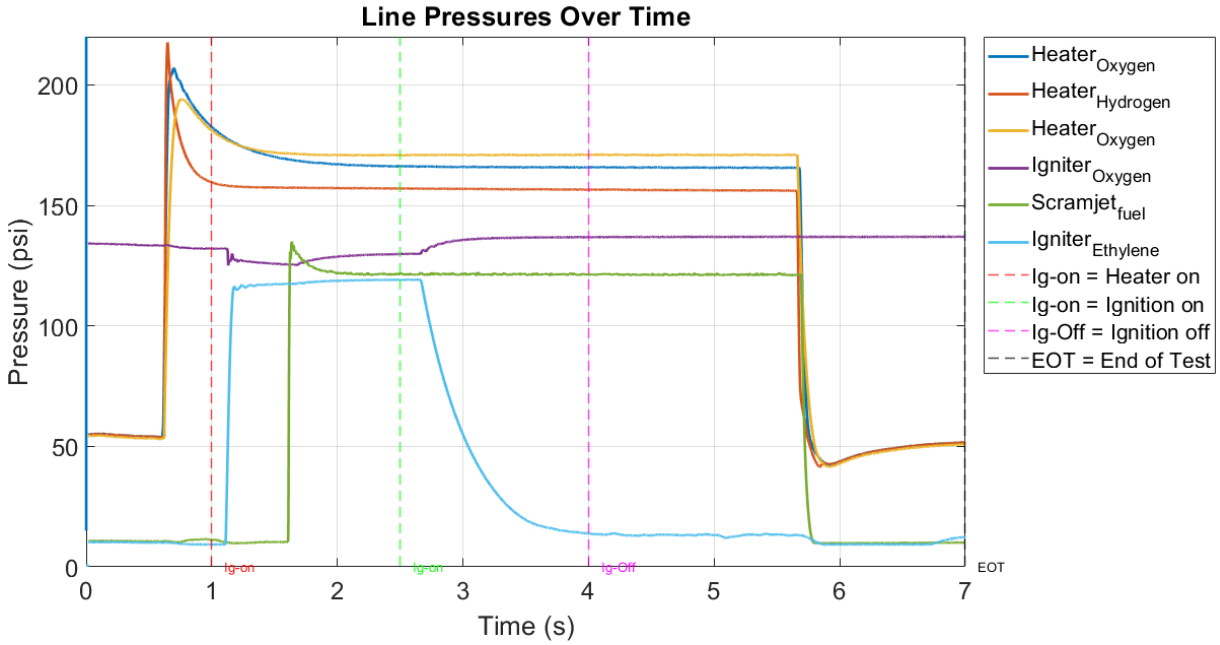

Figure 3.5.1: Typical heater operation and recorded measurements for each test include pressure signatures of the six main gas lines

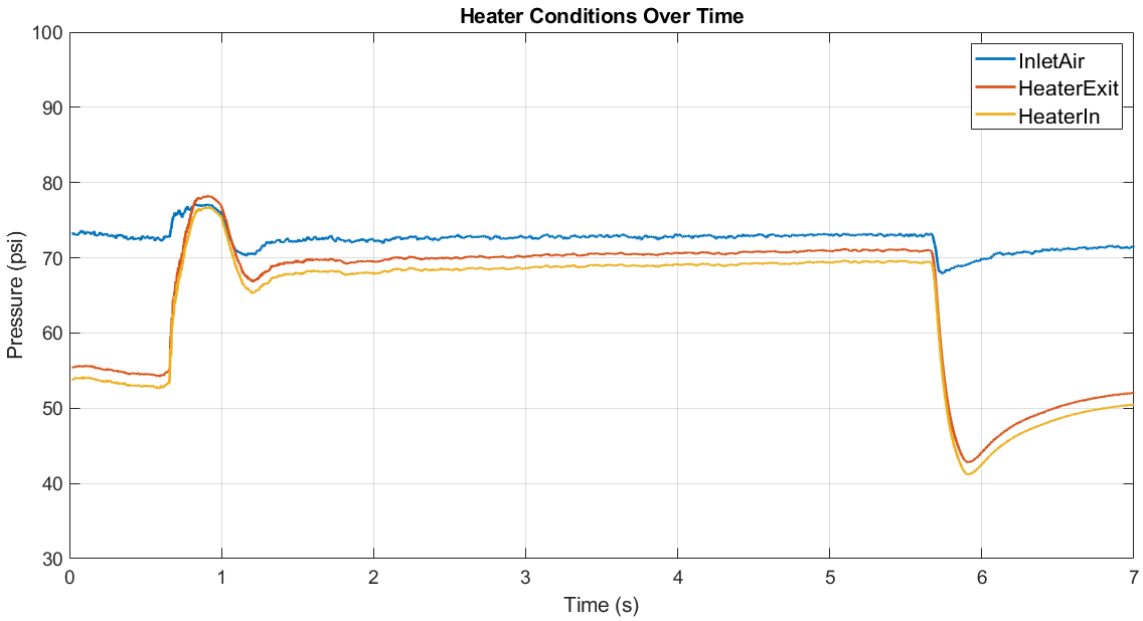

Figure 3.5.2: Typical chamber pressure data

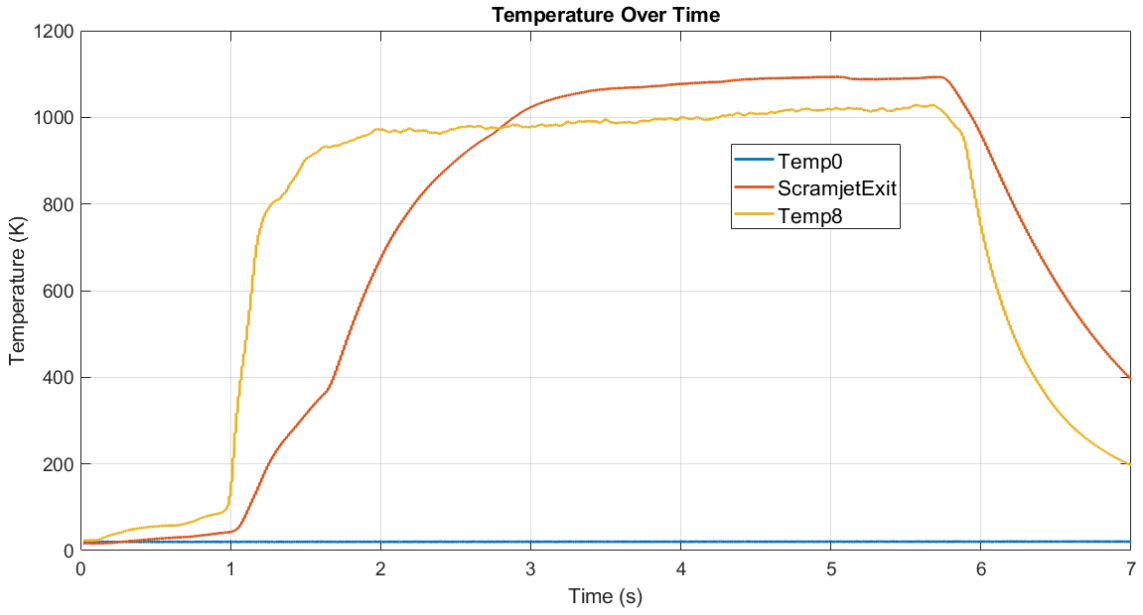

Figure 3.5.3: Typical thermocouple temperature readings (measurement locations are shown in Figure 3.3).

3.4 Diagnostic Techniques

In the scramjet-responding flow studies, static and dynamic pressure measurements and flow diagnostic methods were used. To analyze the responding flow, static wall pressure data along with dynamic pressure data are combined with Schlieren imaging and broadband luminescence pictures. The strategies and procedures used in collecting the data, along with the instrumentation, will be covered in the following sections.

3.4.1 Pressure Measurements

Static pressure measurements are collected at certain locations on the top and lower walls of the scramjet isolator and combustor flow channel. The purpose of these tests was to understand the impact of heat addition on the combustor and determine whether it operated in supersonic or thermally choked mode. Pressure data is measured via a Scanivalve DSA-3217 Digital Sensor Array at a sampling frequency of 500 Hz. The module has 16 temperature-controlled piezoresistive pressure sensors. Scanivalve's DSALink4 software and a desktop PC may connect with the module via TCP/IP and UDP, allowing pressure readings to be acquired and exported as a CSV file for further processing. The sensor array included temperature-compensated piezoresistive pressure sensors, a pneumatic calibration valve, and a range of 0 to 1.5 MPa. Before each test run, a zero offset calibration was done utilizing software and the module's internal calibration valve to address any zero drift concerns caused by piezoresistive sensors.

To dynamically record the pressure changes, a Kistler pressure sensor *(Type: 211B5, Sensitivity: 57.66 mV/psi, Range: 100 psi)* was used due to its high sensitivity, allowing the pressure fluctuations to be captured with a sample rate of 10,000 Hz. To prevent thermal drift

from the high temperatures of the combustion chamber, the Kistler sensor is usually water-cooled. Its installation on the test rig is shown in Figure 3.6.

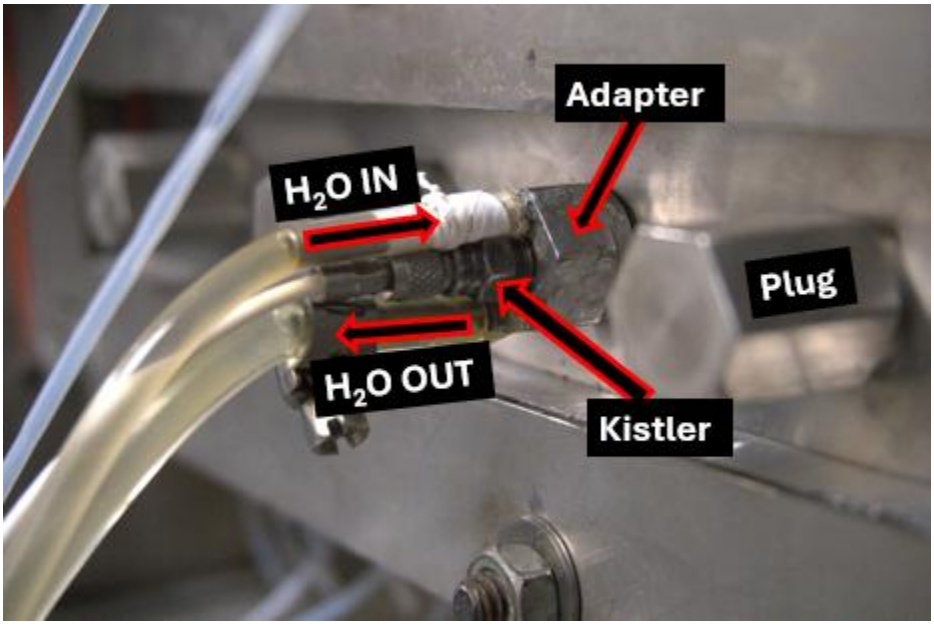

Figure 3.6: Kistler Pressure Sensor mounted to Combustor metal wall (X/H = 5)

The first connection to the sensor was an adapter glued to a metal window. To this end, this adapter consists of two metal tubes that allow water to flow continuously, entering from one end and exiting through the other, such that the Kistler sensor remains cool. Data were acquired by connecting the Kistler sensor to the Kistler station and filtering using a high-pass filter of 5 Hz. It was then processed through a low-pass filter at the Nyquist frequency of the sampling rate (5,000 Hz) recorded by the NI CompactRIO-9022 and saved in a ".lvm" file for analysis.

Chapter 4: Combustion Dynamics and Instability

4.1 Rayleigh's Criterion

A fundamental framework to understand these instabilities is Rayleigh's Criterion, which describes the interaction between pressure fluctuations and heat addition in a compressible flow system. Rayleigh's Criterion can be stated as follows:

"If heat is added to a gas during the phase of greatest compression (i.e., pressure peak), the acoustic oscillations are amplified. Conversely, if heat is added during the phase of rarefaction (i.e., pressure trough), the oscillations are dampened."

In essence, constructive coupling between pressure and heat release fluctuations leads to growth in acoustic energy and, consequently, instability. This is mathematically expressed as in Equation 4.2.1, where the net acoustic energy (ΔE) is equal to the integral of the local pressure fluctuation (P') times the heat release fluctuation (q') as the time (t) goes to the time plus the oscillation period (t+T)

$$\Delta E = \frac{\gamma-1}{\gamma \bar{p}} \int_V \int_t^{t+T} P'(x,t) \cdot q'(x,t)\, dt\, dV \qquad (4.2.1)$$

In our dual-mode scramjet experiments, dynamic pressure measurements and high-speed imaging reveal a pronounced instability at $\boldsymbol{\Phi} \approx 0.24$, with a dominant oscillation at 957 ± 8 Hz (Chapter 4). According to Rayleigh's Criterion, the mean static pressure in the combustor was measured at 10.9 psi (~75.2 kPa), and the amplitude of the pressure fluctuation was 0.2 psi

(~1.38 kPa), corresponding to a 4% fluctuation relative to the peak. Assuming ideal gas behavior with $\gamma = 1.4$, and using a conservative estimate of spatial correlation between pressure and heat release fluctuations (i.e., assuming approximate phase alignment), the energy input due to instability can be approximated. Taking the volume-integrated and cycle-averaged Rayleigh integral as a volumetric energy density, the energy change can be several orders of magnitude above typical background acoustic levels in subsonic or weak compressible flows. The implication is that even a small-amplitude (4%) pressure oscillation when synchronized with unsteady heat release can drive significant instability growth over time.

4.2 Instability in Natural Transition Mode

The dual-mode operation combines scramjet engines (supersonic combustion) with those of ramjets (thermally choked combustion), providing an efficient propulsion system for varying speed conditions. These engines are capable of being optimized to efficiently propel vehicles at high Mach numbers in the typical range of Mach 4 to 10 by dynamically transitioning between these two combustion modes, which is characterized in this experiment by the equivalence ratio through visual observation and data analysis. Yet, one of the most critical obstacles to their development and operation is combustion instabilities. Such instabilities, exhibiting fluctuating pressure, chaotic heat release, and oscillating flow, can greatly degrade engine performance by causing a change in thrust and, in critical situations, cause inlet unstart a sudden airflow breakdown causing total propulsion failure.

To record these short-lived flame dynamics, high-speed imaging was carried out using a high-speed camera with the following conditions: 10,000 frames per second (fps), 99 μs

exposure time, and 1280 × 400 pixels resolution. While the data extraction process was conducted on the entire footage, the analysis was limited to frames 25,000 to 35,000, corresponding to the time region when the engine is predicted to reach steady-state operation post-igniter shutdown. Under several conditions, the dual-mode scramjet was either operating deep within the thermally choked mode or entrenched in the supersonic combustion mode, the cavity-stabilized flame was found to remain stable for the duration of the test (as seen in Figure 4.1, where the engine is in supersonic mode, and Figure 4.2, where the engine is in thermally choked mode). Under the transition equivalence ratio regime ($\boldsymbol{\Phi}$ of 0.24 - 0.3), a sudden and abrupt flame motion occurs immediately after the scramjet igniter is cut off. In some cases, these flame fluctuations can be very swift, while some can even continue for the duration of the test, as illustrated in Figure 4.3.

The observations highlight the critical nature of the transition regime in dual-mode scramjet combustion, where instabilities can emerge due to variations in flame anchoring mechanisms and heat release. These instabilities significantly impact the stability and performance of the combustor flow field, posing challenges to the reliable operation of dual-mode scramjets. Understanding and mitigating these instabilities are essential for ensuring consistent performance in hypersonic applications.

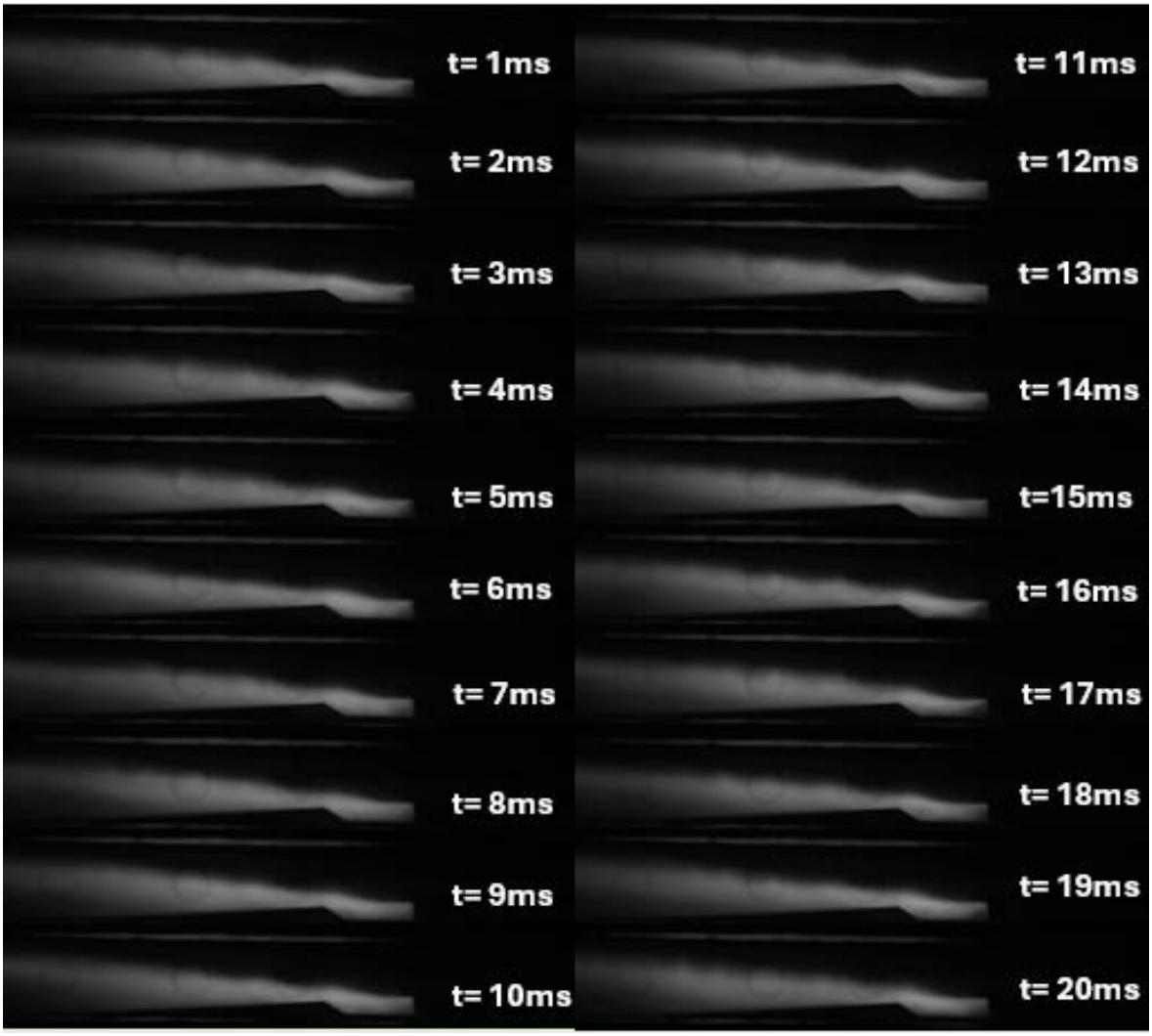

Figure 4.1: High-speed camera sequence of the event for Φ = 0.13 (Steady Supersonic combustion mode)

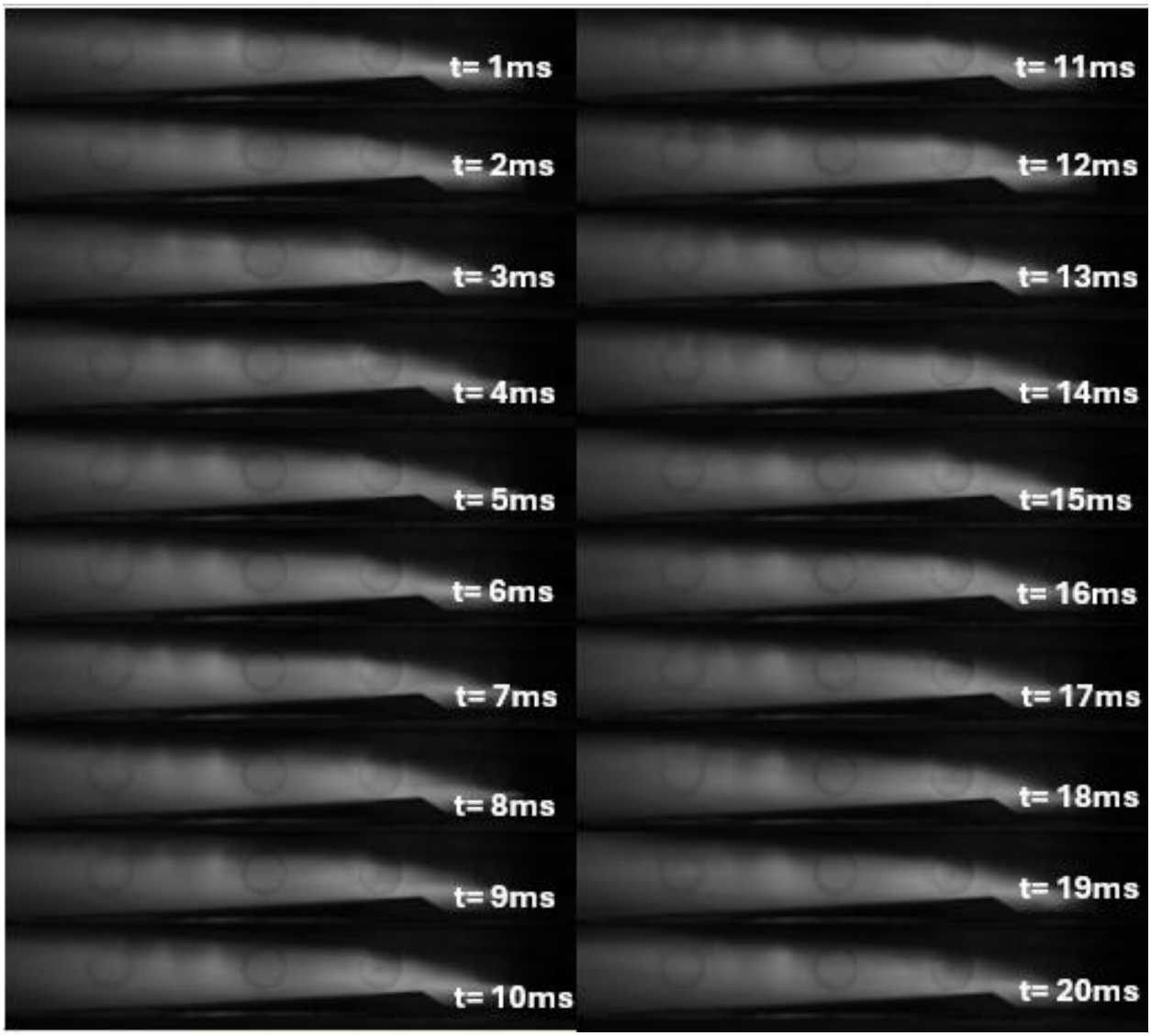

Figure 4.2: High-speed camera sequence of the event for Φ = 0.31 (Steady Thermally choked combustion mode)

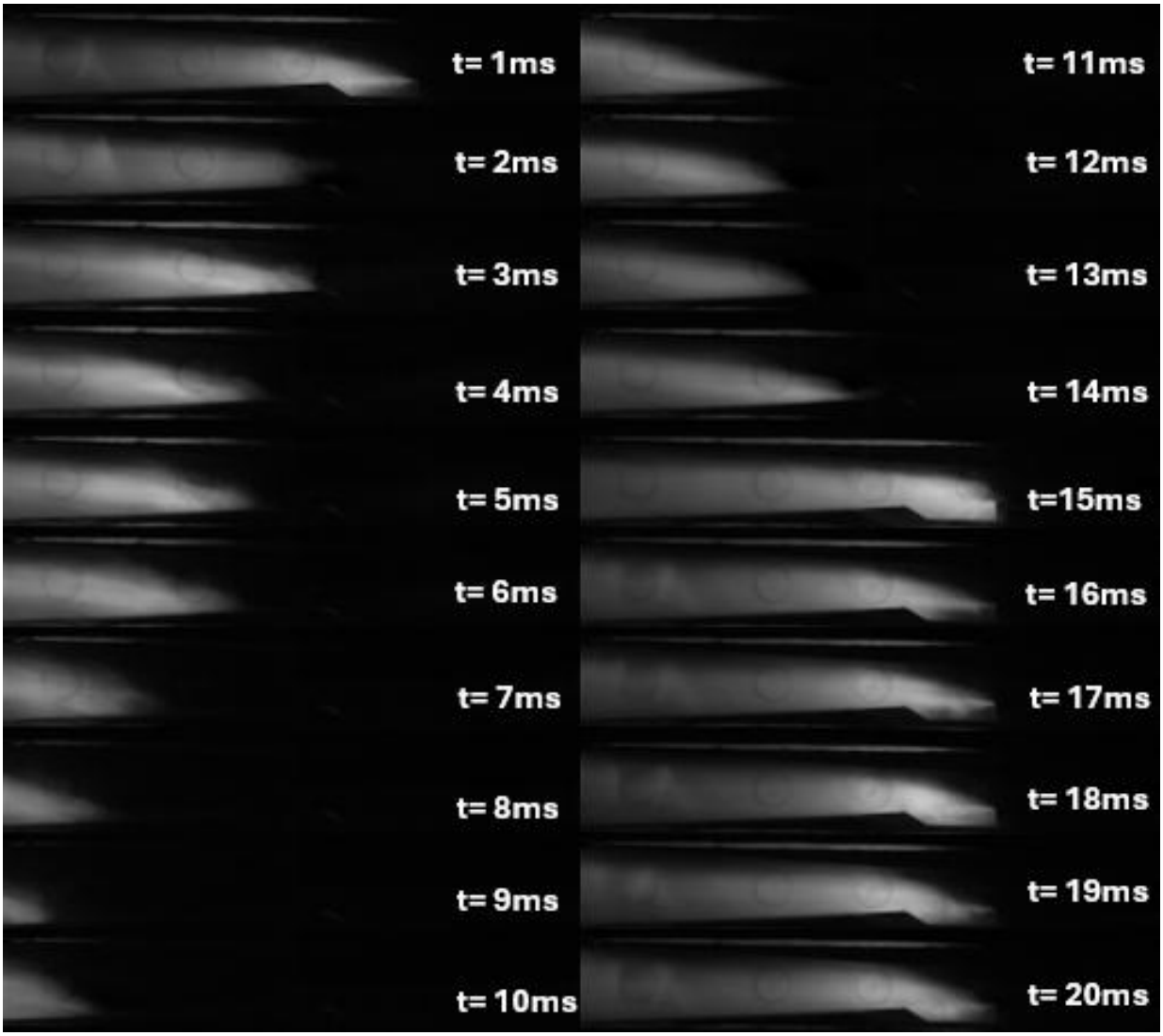

Figure 4.3: High-speed camera sequence of the event for $\Phi = 0.28$ (instability)

To better characterize these phenomena, Figure 4.4 presents the scanivalve pressure measurements at the port at the leading edge of the cavity, illustrating the pressure oscillations over time. These oscillations provide insight into the dynamic behavior of the combustor and the transition between combustion modes.

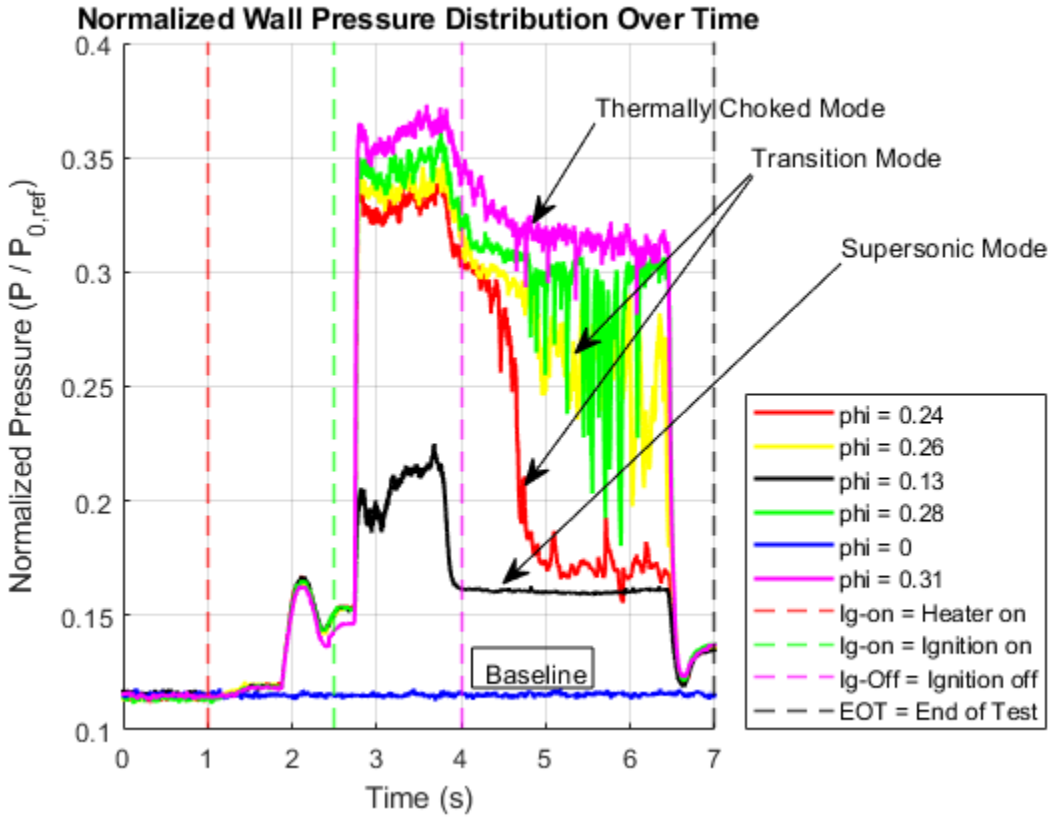

Figure 4.4: Plot of Static pressure vs time at the port in the leading edge of the cavity (x/H = 1)

To investigate combustion instabilities in the dual-mode scramjet engine, a Kistler pressure sensor was used to measure dynamic pressure fluctuations in the combustion region. These measurements were analyzed to identify dominant frequency components and assess their impact on combustion stability. After applying a Hanning filter and performing a Fast Fourier Transform (FFT) on the pressure data, the highest peak was observed at an equivalence ratio ($\boldsymbol{\Phi}$) of 0.24, as shown in Figure 4.5. This indicates that the flame was attempting to thermally choke, leading to oscillatory behavior in the flow. For conditions where combustion was purely supersonic ($\boldsymbol{\Phi} < 0.24$) or fully thermally choked ($\boldsymbol{\Phi} > 0.3$), the FFT analysis revealed no dominant frequency components, suggesting stable operation in these regimes. However, in the transitional regime ($0.24 \leq \boldsymbol{\Phi} \leq 0.3$), clear harmonic peaks were identified specifically at 957 ± 8 Hz for the first harmonic and 1914 ± 8 Hz for the second harmonic within the steady-state period, as shown in Figures 4.6, 4.7, and 4.8.

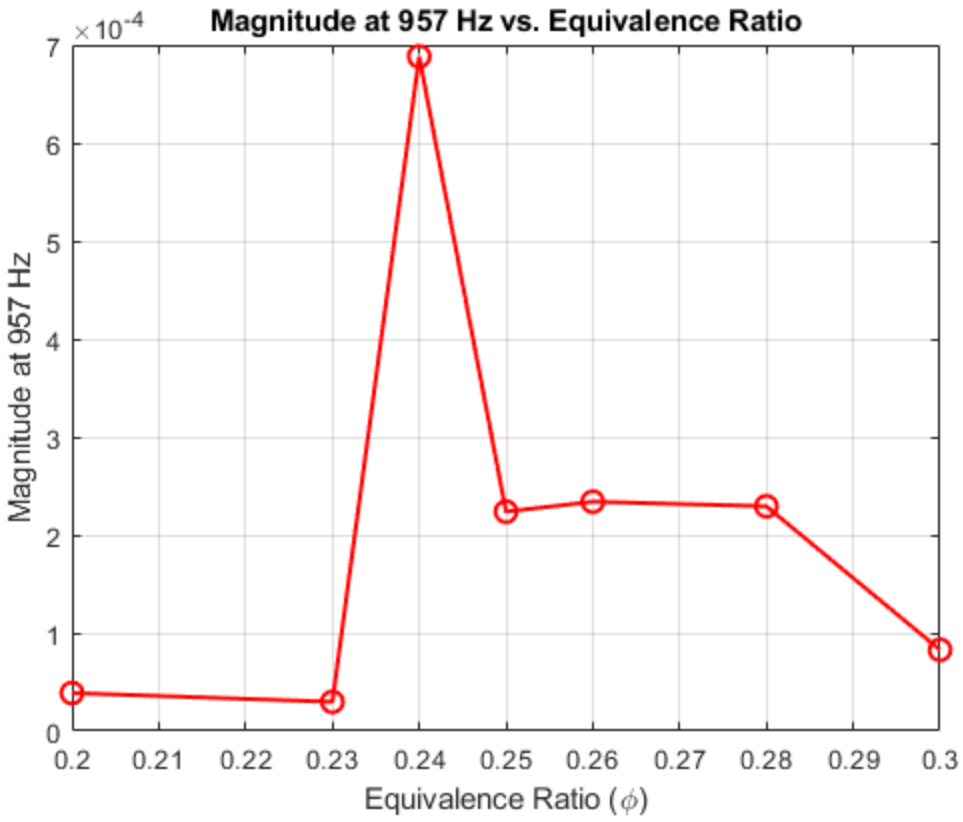

Figure 4.5: Plot of Frequency Magnitude at 957 Hz for different $\boldsymbol{\Phi}$ *values*

Among these cases, $\boldsymbol{\Phi}$ = 0.24 exhibited the most pronounced peak, confirming it as the critical transition point where combustion instability was most intense. This is illustrated in Figure 4.9, which highlights the onset of significant fluctuations associated with the transition to thermal choking. The combustion process undergoes instability due to the interaction of shock waves, boundary layers, and heat release. Understanding these oscillations is crucial for optimizing scramjet performance.

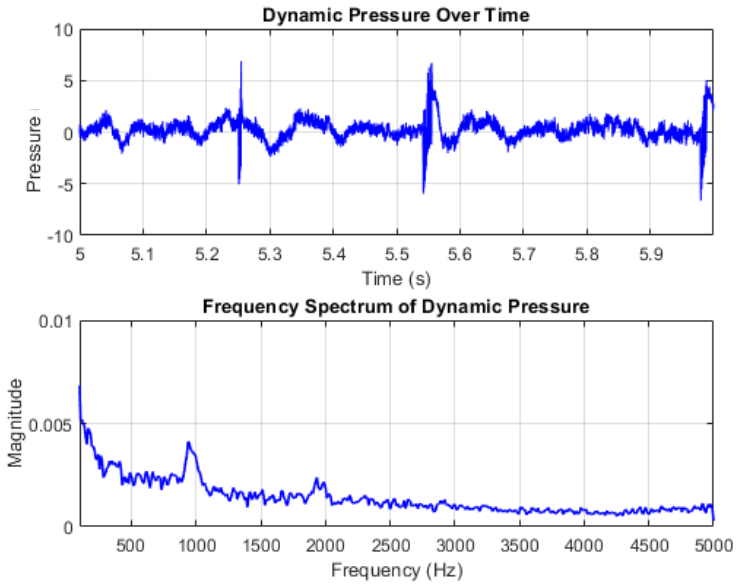

Figure 4.6: Plot of Dynamic pressure vs time and FFT for $\Phi = 0.25$

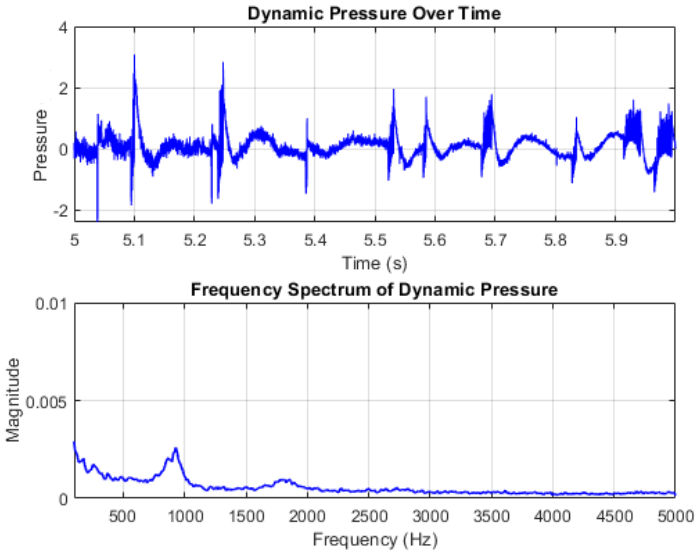

Figure 4.7: Plot of Dynamic pressure vs time and FFT for $\Phi = 0.3$

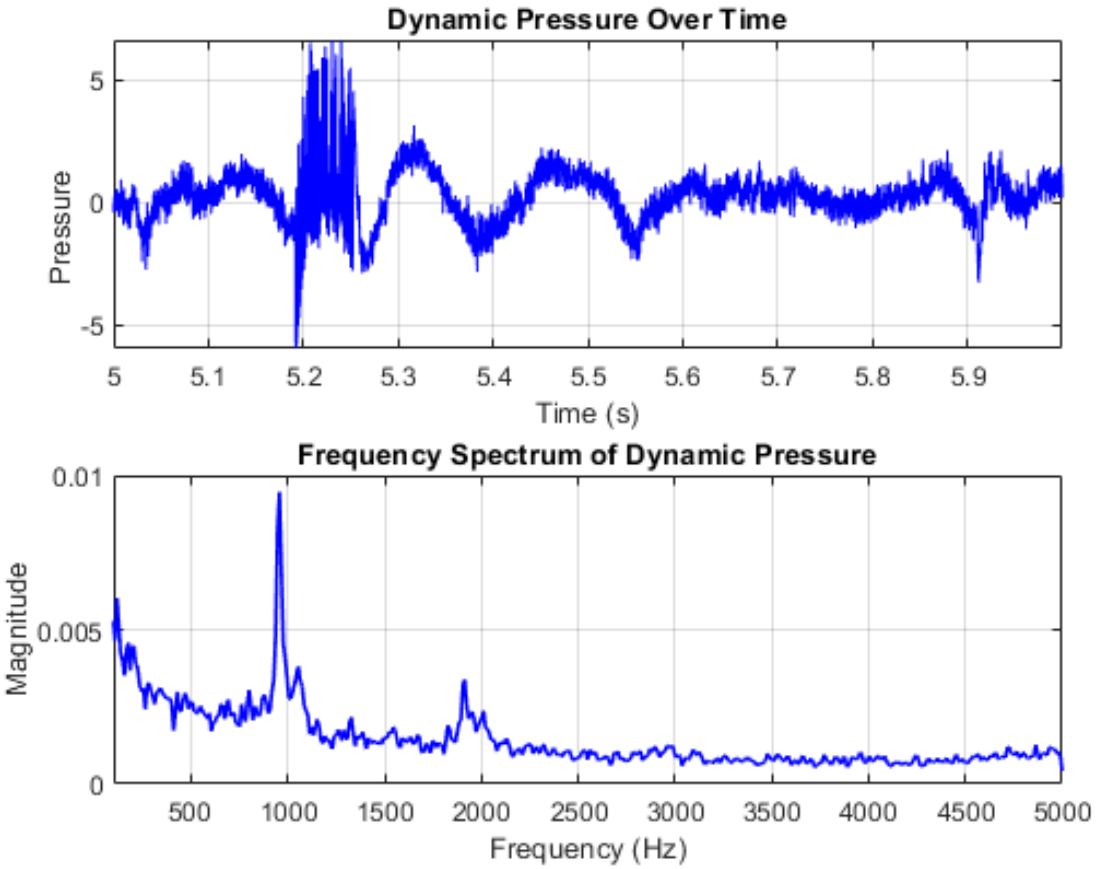

Figure 4.8: Plot of Dynamic pressure vs time and FFT for $\boldsymbol{\Phi} = 0.24$

To confirm this dominant frequency is not false, the data for $\boldsymbol{\Phi}$ at 0.24 was run through a high-pass filter at a frequency equal to the first harmonic frequency and then, DC drift was removed. This will isolate that frequency, as shown in Figure 4.9. Then, to further confirm the presence, the data was zoomed in at one of the isolated frequencies to count the period, which confirmed the presence of the 957 Hz frequency shown in Figure 4.10. Lastly, for better visualization, the spectrogram was plotted in both 3D and 2D, as shown in Figures 4.11 and 4.12.

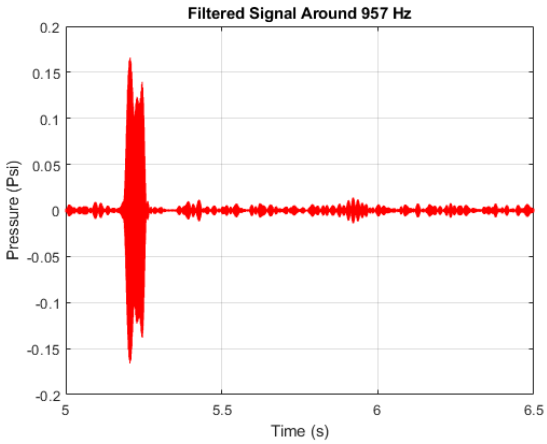

Figure 4.9: Plot of dynamic pressure data of $\Phi = 0.24$ *through a high-pass filter*

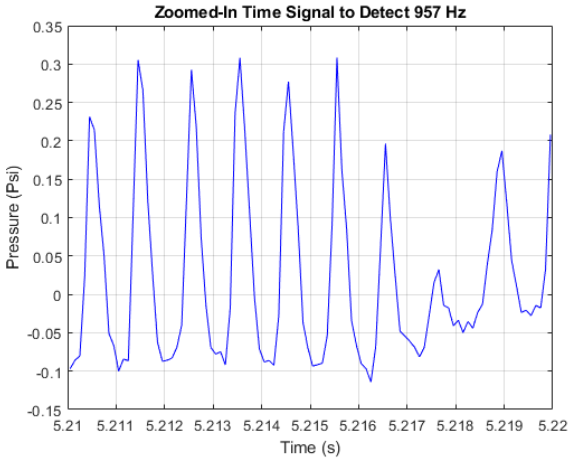

Figure 4.10: Plot of dynamic pressure data of $\Phi = 0.24$ *to confirm presence of 957 Hz*

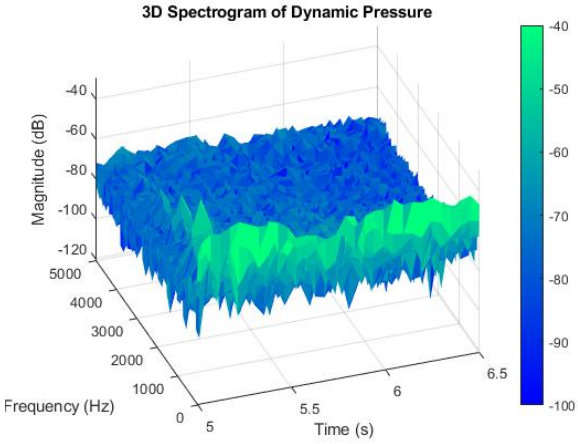

Figure 4.11: 3D Plot of dynamic pressure data Spectrogram at $\Phi = 0.24$

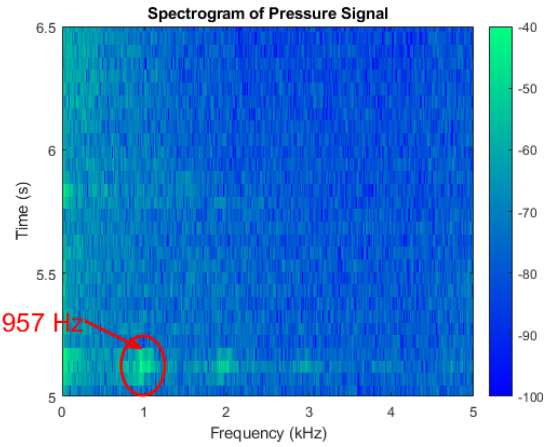

Figure 4.12: 2D Plot of dynamic pressure spectrogram at $\Phi = 0.24$

The analysis of pressure fluctuations at 957 ± 8 Hz provides critical insights into combustion instability and the transition equivalence ratio. The filtered time-domain signal reveals how pressure oscillations evolve, with sustained high-amplitude oscillations indicating thermoacoustic coupling, which reinforces instability. A zoomed-in view further clarifies whether the oscillations are periodic (single-mode instability) or irregular, suggesting mode switching in the combustion process. The spectrogram provides a time-frequency representation, showing how the 957 ± 8 Hz component persists or grows over time. This frequency remains dominant across all $\boldsymbol{\Phi}$ values, which suggests a resonant instability mode, whereas the emergence of multiple frequencies indicates a transition between different combustion regimes. Instability typically increases with $\boldsymbol{\Phi}$ until reaching a critical transition point, where the system exhibits peak instability before either stabilizing at richer mixtures or entering a chaotic state. Then, the instability weakens at a high $\boldsymbol{\Phi}$ value, which suggests a stabilizing effect of increased reactant availability, reducing acoustic coupling. Overall, this analysis helps determine optimal operating conditions where stable combustion is maintained, preventing unwanted instability that could lead to flame blowout or efficiency loss.

Based on the sensitivity of the Kistler pressure sensor used, the dynamic pressure at the trailing edge of the cavity was measured to be about 0.2 psia, and the wall pressure at that location was measured to be 10.9 psia. The calculated pressure fluctuation is approximately 2% from average pressure, indicating a significant deviation from the static wall pressure at the measurement location. This level of fluctuation suggests the presence of strong unsteady flow behavior, likely driven by combustion-induced oscillations. In the context of the scramjet combustor, such a high percentage of pressure variation is a clear indicator of thermoacoustic instability, particularly within the transition regime identified in previous chapters. These

fluctuations not only disrupt steady combustion but also interfere with efficient energy conversion, contributing to thrust degradation. The magnitude of this fluctuation further supports the conclusion that the 957 ± 8 Hz frequency peak observed in spectral analyses is tied to a resonant instability mode amplified by Rayleigh-type feedback between pressure and heat release.

Chapter 5: Effect on Performance Matrix (Thrust)

Thrust generation in a dual-mode scramjet engine is highly sensitive to the stability of the combustion process. Combustion instabilities, characterized by pressure fluctuations, unsteady heat release, and acoustic feedback, significantly impact the engine's performance matrix, including thrust, specific impulse, and efficiency. A key frequency component at 957 ± 8 Hz has been identified as a dominant instability mode, revealing crucial insights into the behavior of the engine across different $\boldsymbol{\Phi}$. This chapter explores how combustion instability affects thrust production.

5.1 Effects on Engine Thrust

Combustion instability in a dual-mode scramjet significantly affects thrust generation due to the complex interplay between pressure fluctuations, heat release dynamics, and acoustic feedback. At 957 ± 8 Hz, dominant pressure oscillations indicate thermoacoustic coupling, where pressure waves reinforce unsteady combustion, leading to thrust fluctuations. In the supersonic combustion mode at low equivalence ratios ($\boldsymbol{\Phi} < 0.24$), the flame remains stable, thrust output is steady, and the pressure is not as high as in the thermally choked mode initially. Thus, as $\boldsymbol{\Phi}$ increases toward the transition regime ($0.24 \leq \boldsymbol{\Phi} \leq 0.30$), instability intensifies, causing large thrust oscillations due to the modes changing between low and high pressure indicated by the transient flame movement, and potential inlet unstart all of which disrupt the propulsion system’s reliability, this phase exhibits strong resonant instability, where the energy from combustion is inefficiently transferred to propulsion due to increased acoustic coupling. As the equivalence ratio rises further ($\boldsymbol{\Phi} > 0.30$), the instability weakens, suggesting that higher fuel availability reduces pressure oscillations, improves combustion steadiness, and restores thrust stability, and

the overall combustion pressure is at its maximum. Figure 5.1.1 shows the wall pressure distribution vs. distance for a fully supersonic ($\boldsymbol{\Phi}$ = 0.13) and thermally choked case ($\boldsymbol{\Phi}$ = 0.43) and for a case in the transition regime ($\boldsymbol{\Phi}$ = 0.24).

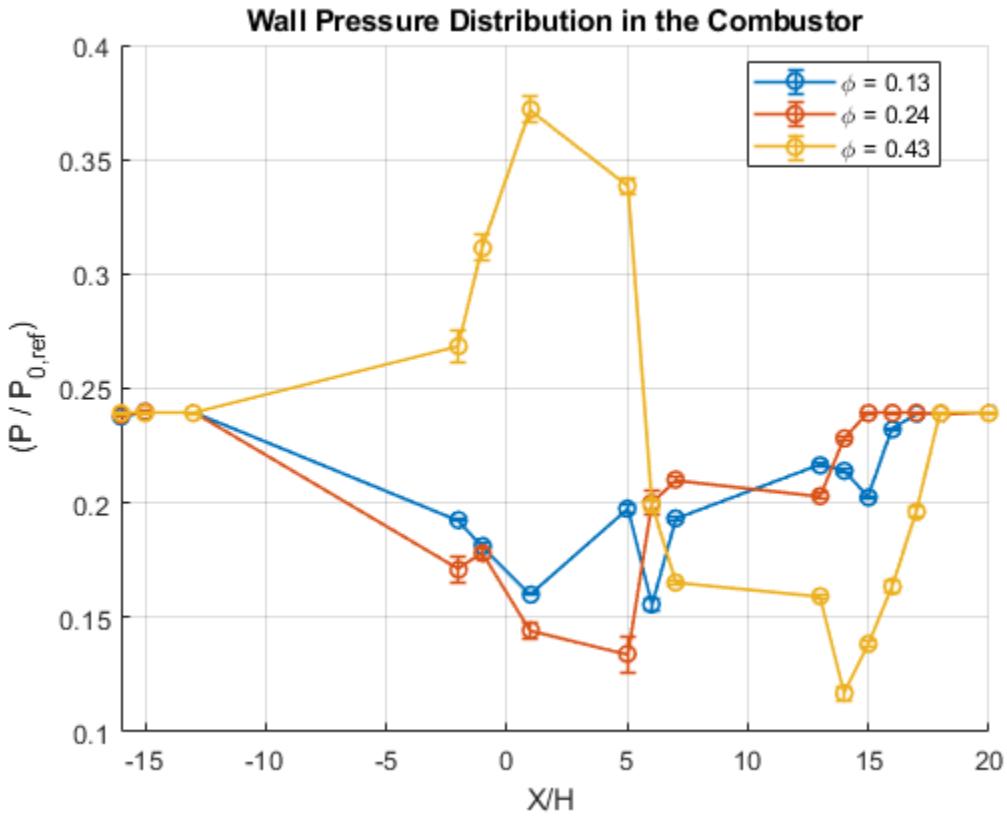

Figure 5.1.1: Plot of normalized wall pressure vs. normalized distance (X/H) along the combustor

The overall effect of instability on thrust performance is a decrease in net thrust, as the energy otherwise converted into directed exhaust momentum is instead lost to sustaining

pressure waves. This highlights the importance of controlling combustion instability to maintain consistent and efficient thrust output in scramjet engines.

The spectral analysis of dynamic pressure fluctuations from Chapter 4 provides crucial insights into how combustion instability affects thrust performance in a dual-mode scramjet engine. The FFT analysis reveals a dominant 957 ± 8 Hz instability mode, which persists across different $\boldsymbol{\Phi}$. This frequency remains strongest during the transition regime, where high-amplitude oscillations indicate severe thermoacoustic coupling, leading to significant thrust unsteadiness. Before this unsteadiness (combustion in full supersonic mode), the thrust is relatively stable. During the peak instability phase, additional frequency components emerge, suggesting mode-switching behavior and chaotic thrust variations, which can lead to inlet unstart or flame blowout. By comparing thrust output in different stability conditions using Mithuun's data [12], where he measured the velocity in the combustor using the 2-Point Focused Laser Differential interferometry (2pFLDI) velocimetry technique. It is observed that thrust decreases by up to 3.5% locally when instability is initiated, demonstrating a direct link between pressure oscillations and thrust degradation as shown in Figure 5.1.2, which will grow as instability increases. Equation 5.1.1 shows the relationship between local thrust and pressure oscillations. Using the measured local velocity from Mithuun's experiment, we are able to plot pressures collected within the steady-state time when the combustor is in full supersonic mode and full thermally choked mode and use that in Equation 5.1.1 to see the local thrust oscillation due to the oscillating pressure as the natural transition mode will go between supersonic mode and thermally choked mode several times.

$$T(x) = p(x)A(x) + \dot{m}U(x) \tag{5.1.1}$$

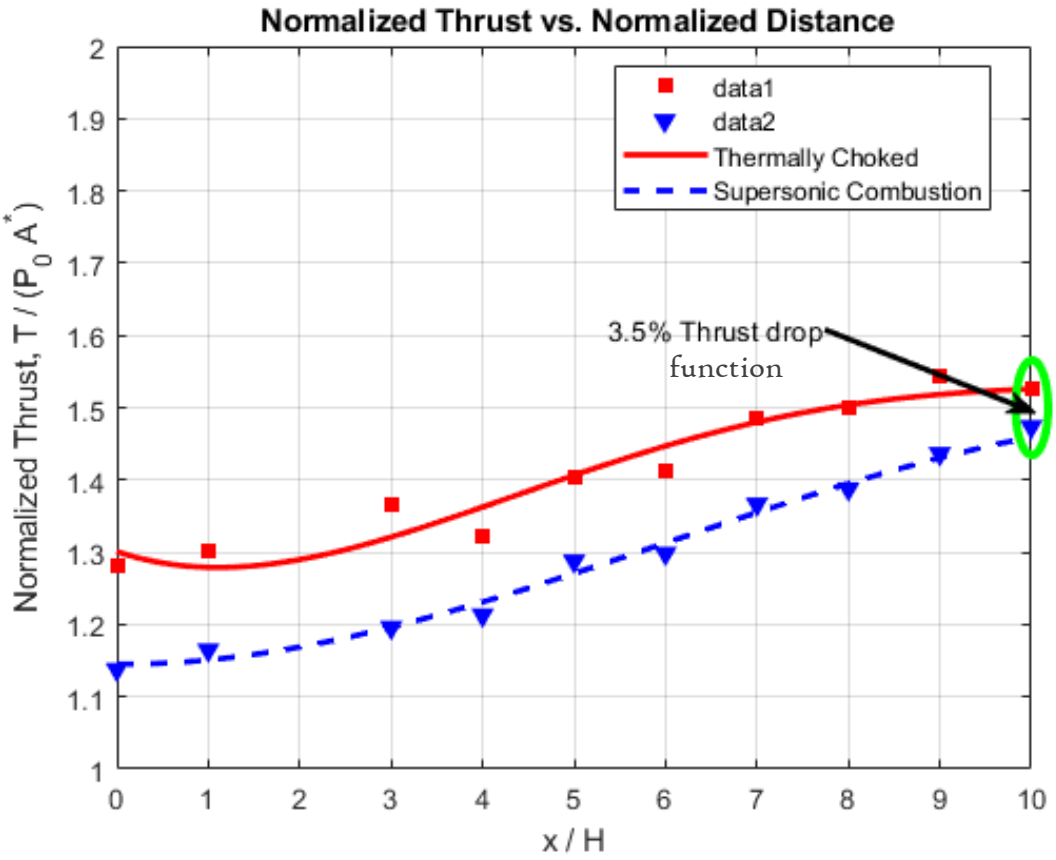

Figure 5.1.2: Plot of the effect of pressure oscillation on the engine's local thrust at X/H = 10

The total thrust drop due to pressure fluctuations in a scramjet combustor was analyzed, which supports the above findings. It compares the two operating modes. Using measured exit velocities and combustor exit temperatures, the code calculates the Mach number at the end of the combustor, using the Mach-area relation shown in Equation 5.1.2, and solves for the nozzle

exit Mach number using the Mach-area relation also. It then determines the corresponding exit temperature, velocity, and density to evaluate thrust using Equation 5.1.3.

$$\frac{A}{A^*} = \frac{1}{M}\left(\frac{2}{\gamma+1}\right)^{\frac{\gamma+1}{2(\gamma-1)}}\left(1+\frac{\gamma-1}{2}M^2\right)^{\frac{\gamma+1}{2(\gamma-1)}} \quad (5.1.2)$$

$$T = (\rho_e U_e A_e)U_e - (\rho_\infty U_\infty A_\infty)U_\infty + (P_e - P_\infty)A_e \quad (5.1.3)$$

In the single injector case (thermally choked), a perfectly expanded nozzle is assumed ($P_e=P_\infty$), maximizing thrust. In the distributed case (supersonic mode), the flow is under-expanded ($P_e>P_\infty$), introducing a pressure mismatch penalty. The results show a ~13.5% decrease in thrust in the distributed case, directly linking the experimentally observed pressure drop to reduced momentum and pressure thrust. Thus, pressure fluctuations during combustion mode transition have a measurable and significant impact on scramjet performance.

5.2 Strategy for Avoiding Natural Transition Mode

To mitigate the challenges associated with the natural transition in dual-mode scramjet engines, an active control strategy involving distributed fuel injection can be implemented. This method aims to delay the onset of thermal choking by ensuring a more gradual and controlled heat release distribution within the combustor. As discussed in Mithuun's work [12], active control is achieved through a combination of fuel scheduling and distributed injection, allowing seamless transitions between thermally choked and supersonic combustion modes. Unlike

conventional scramjet configurations where fuel is injected at a single point, this method utilizes four spatially distributed injectors. By dispersing the heat release across a larger volume rather than concentrating it at a single location, the combustor is less prone to premature choking. For instance, if single-point fuel injection results in thermal choking at a Φ of 0.31, distributing the same fuel mass across multiple injectors enables the system to sustain higher Φ values before choking occurs. It is significantly better to go through the transition mode and maintain the mode of transition compared to passing through the natural transition, which switches from one mode to the other several times before one mode is maintained. This active control strategy provides the flexibility to modulate between single and distributed injection, effectively maintaining stable operation across different combustion regimes. By dynamically adjusting the injection configuration in real-time, the system can suppress abrupt transition events that lead to combustion instabilities, inlet unstart, and reduced performance. Figure 5.2.1 illustrates the fuel distribution strategy within the combustion chamber, demonstrating how this method enhances stability and prevents unwanted natural transitions.

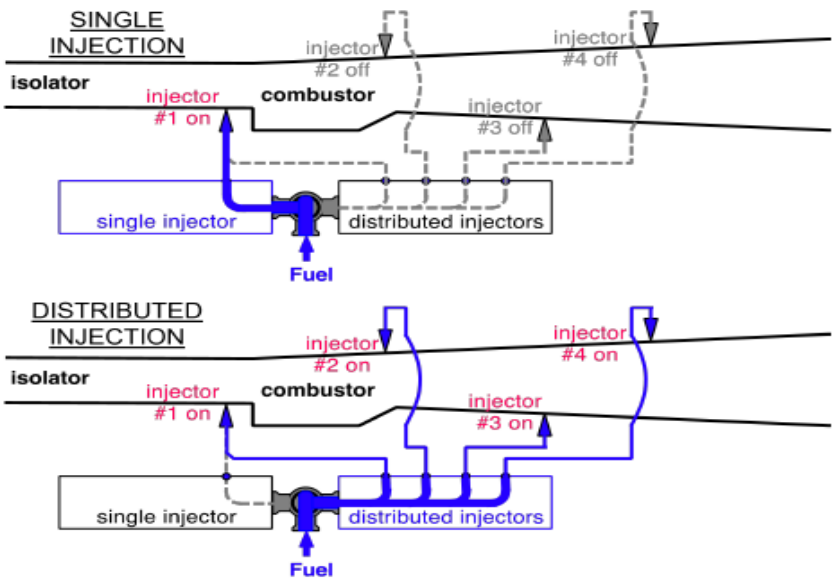

Figure 5.2.1: Single injector case vs Distributed injector case for an active control sequencing [12]

To maintain optimal thrust when transitioning from thermally choked mode (using a single injector) to supersonic combustion mode (using four injectors), the engine must operate at a Φ greater than 0.31. At Φ = 0.31, the system shifts to distributed injection, but at a higher Φ while remaining within the supersonic combustion regime (Φ < 0.52). Assuming the transition equivalence ratio for distributed injection occurs at $0.524 \leq \Phi \leq 0.6$, this strategy ensures that the engine avoids natural transition-induced instabilities while sustaining efficient thrust generation. Figure 5.2.2 illustrates how this approach enables a smooth transition from single injection to distributed injection, optimizing both stability and performance.

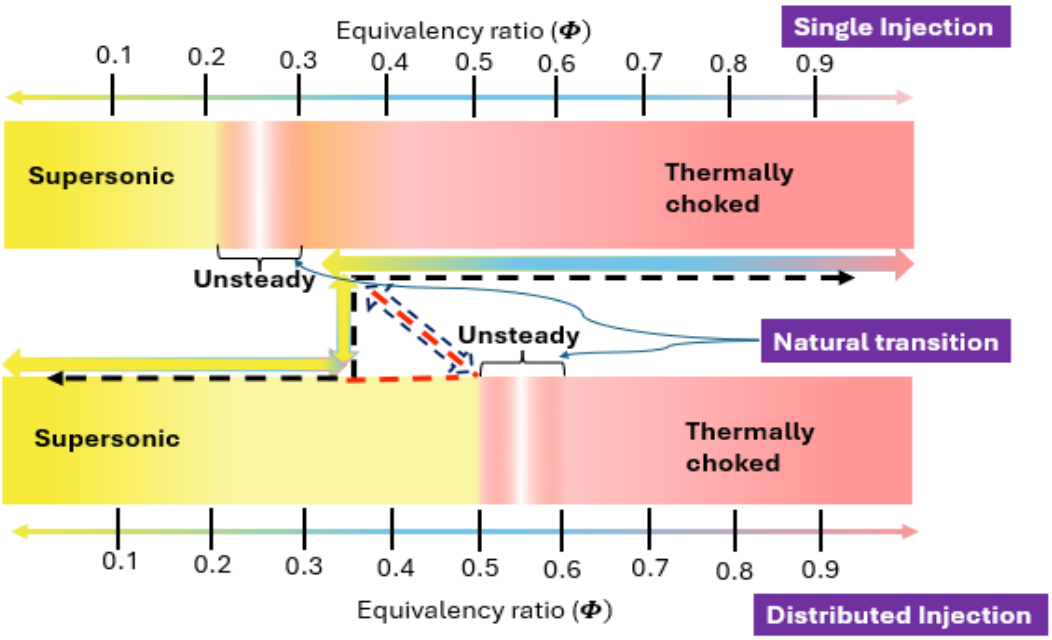

Figure 5.2.2: Strategy for controlling stable transitioning between thermally choked mode and supersonic mode

By doing this, there will be a drop in thrust. However, this drop occurs once, and the effect is not as significant as going through the natural transition regime to change between combustion modes. Ultimately, this strategy provides a practical and effective framework for enabling real-time control of mode transitions, enhancing both the performance and reliability of dual-mode scramjet engines operating over a wide range of flight conditions.

Chapter 6: Conclusion

The effects of mode transitions on scramjet engine performance were investigated using a dual-mode ramjet-scramjet model combustor. Combustion experiments were conducted at the University of Maryland's vitiated airflow facility, which simulated Mach 5 flight conditions by mixing combustion products with oxygen-enriched air to match the enthalpy and oxygen concentration of real atmospheric conditions. The two-dimensional model combustor featured a flame-holding cavity to support stable combustion and a six-degree area expansion in the transverse direction to accelerate the supersonic reacting flow.

To characterize the flow field and evaluate combustor performance metrics, a combination of static wall pressure measurements along the axial direction using a rapid-pressure-scanner system, combustor pressure fluctuation measurements using high-frequency-response dynamic pressure transducers, and high-speed flow visualization diagnostics was employed. The baseline configuration with a single-point hydrogen fuel injection was used for combustion experiments over a range of equivalence ratios ($\boldsymbol{\Phi}$) to determine the critical equivalence ratio for natural mode

transition. These series of combustion experiments and experimental data-based cycle analysis formed the foundation for quantitatively assessing the effects of combustion mode transition on combustion instability and thrust modification results presented in Section 6.1.

6.1 Key Findings

This study has provided significant insights into the effects of mode transition on combustion instability and thrust performance in a dual-mode ramjet-scramjet engine and demonstrated how fuel distribution control strategies may be used to mitigate the adverse effects

of natural mode transition. The dynamic pressure measurements showed coherent oscillations at 957 Hz. The results showed that the thermoacoustic instabilities are present when the combustor is operating at fuel-air ratios close to the point of natural combustion mode transition. When the combustor is operating at an equivalence ratio ($\boldsymbol{\Phi}$) below 0.2, the combustion mode remains supersonic and stable, with no evidence of combustion instabilities. However, as $\boldsymbol{\Phi}$ approached the critical equivalence ratio, pressure oscillations intensified, reaching their peak amplitude at $\boldsymbol{\Phi} \approx 0.24$. Also, significant flame movements were observed at these conditions. Above $\boldsymbol{\Phi}$ of 0.30, the combustor again becomes stable, but now operating in a thermally choked mode. No instability was observed at higher equivalence ratios tested. This confirms that combustion instabilities are associated with the combustion mode transitions. In a naturally induced combustion mode transition process, as the combustion mode shifts back and forth between the two modes, wild flame movements are observed and pressure oscillations couple with heat release leading to combustion instabilities. Another key finding is that the effect of mode transition on uninstalled thrust is substantial. By performing cycle analysis based on the experimental data and a theoretical nozzle, it was possible to quantify the effect on thrust. When combustion mode transitions from thermally choked mode to supersonic combustion mode, it was revealed that the thrust can decrease as much as 13.5%. The results suggest that such a large change in thrust level can also present serious challenges to the overall engine operability, especially if a natural mode transition process occurs over an extended period of time, while the modes switching back and forth over a duration on the order of 500 msec as suggested by previous studies (Aguilera). The present findings show that the effects of combustion mode transition on combustion instabilities and uninstalled thrust can be substantial, and hence, it may be important to address potential mitigation strategies. Previously, an active control approach of

regulating fuel injection distribution was proposed as an effective strategy of scheduling combustion mode transition while avoiding uncontrolled mode transitions back and forth over a prolonged duration. The effect of distributed fuel injection in controlling mode transitions and preventing abrupt shifts between supersonic and thermally choked combustion has been demonstrated. An additional control strategy has been proposed in this thesis where fuel-air ratio may be adjusted with controlling fuel distribution in such a way to reduce the amount of thrust change associated with

mode transition. Unlike single-point fuel injection which causes transition at relatively low equivalence ratios around $\boldsymbol{\Phi} \approx 0.24\sim0.30$, distributed fuel injection allows the combustion mode transition at higher equivalence ratios around $\boldsymbol{\Phi} \approx 0.52\sim0.60$. The proposed method is to adjust the combustor operation from the single fuel injection at $\boldsymbol{\Phi} = 0.35$ (thermally choked mode; stable) to the distributed fuel injection at $\boldsymbol{\Phi} = 0.45$ (supersonic combustion mode; stable) for a controlled mode transition. By spreading the heat release across multiple injectors and increasing the amount of fueling, this method may avoid the zone of combustion instabilities and may reduce the amount of thrust change associated with natural mode transitions. The ability to modulate between single and distributed injection provided a way to maintain stable combustion across different operating regimes, demonstrating the effectiveness of active control strategies in optimizing thrust performance. The ability to modulate between single and distributed injection provided a way to maintain stable combustion across different operating regimes, demonstrating the effectiveness of active control strategies in optimizing thrust performance.

6.2 Technical Contribution

This research makes several technical contributions to the field of hypersonic propulsion and scramjet instability control in the following ways:

- ➢ This study verified, for the first time, the presence of large-amplitude coherent pressure oscillations (i.e., combustion instability) during the natural combustion mode transition. The results confirm that combustion instability may be a serious risk during mode transition.
- ➢ The FFT analysis of the dynamic pressure measurements show that the peak frequency was centered around at 957 ± 8 Hz and the peak-to-peak amplitude was 4% of the mean.
- ➢ A cycle analysis was conducted using experimental data and a theoretical nozzle. The results revealed a thrust change of more than 13 % associated with the combustor mode transition.

6.3 Future Work

The study on combustion instability and active control methods in dual-mode scramjets has provided valuable insights, but several areas remain unexplored. One key direction for future research is to examine how dynamic pressure spectra react to actively controlled mode transitions, as it is unclear how active control sequencing modifies these pressure characteristics. A detailed spectral analysis of actively controlled transitions implementing the strategy discussed in Chapter 5 could help determine whether instability modes are suppressed, shifted, or intensified, providing valuable information on optimizing transition stability. Furthermore, the refinement and optimization of active control sequencing to make it more applicable in real-world hypersonic flight conditions is crucial. Distributed fuel injection can help regulate combustor mode transitions, but the method must be further developed to account for varying flight conditions, fluctuating inlet disturbances, and real-time control requirements. Investigating

adaptive fuel injection strategies, such as machine learning-driven predictive control algorithms, could enhance the system's robustness and allow it to dynamically adjust fuel scheduling in response to real-time pressure and velocity fluctuations. Another key research focus should be quantifying heat release for different fuel distribution schemes using advanced diagnostic techniques. Preliminary studies have demonstrated the potential of blended hydrocarbon fuels in a dual-mode scramjet combustor, and the use of formaldehyde PLIF (Planar Laser-Induced Fluorescence) in burner experiments could help improve our understanding of energy distribution and thermal choking thresholds in scramjets.

Appendix A: Calculating Equivalency Ratios for the Vitiated Heater Facility

Once the orifice sizes were determined, we calculated the mass flow rate of each gas using the choked flow equation. This equation is suitable for compressible flow through a small orifice under the assumption that the flow becomes sonic at the throat (i.e., choked). The mass flow rate is calculated using the stagnation pressure P_0, the orifice area A, the gas constant R, and the specific heat ratio γ of the gas, as shown in Equation A.1:

$$\dot{m}_{choked} = \frac{P_o \cdot A}{\sqrt{T_O}} \cdot \sqrt{\frac{\gamma}{R}} \cdot \left(\frac{2}{\gamma+1}\right)^{\frac{\gamma+1}{2(\gamma-1)}} \quad \text{(A.1)}$$

From combustion chemistry, the simplified stoichiometric reaction for hydrogen and oxygen is:

$$H_2 + 0.5O_2 \leftrightarrow H_2O$$

However, in our vitiated air facility, we must ensure that the oxygen content in the post-combustion products is restored to 21% by mole. This is to ensure that the air entering the scramjet reflects typical atmospheric oxygen content. To achieve this, we replenish oxygen after the heater combustor. The resulting chemical equation becomes:

$$H_2 + \left(\frac{1}{2}\right)O_2 \leftrightarrow H_2O + \left(\frac{0.21}{0.79}\right)O_2 \quad \rightarrow$$

$$ADDING\ O_2\ Replenishment$$

$$H_2 + 0.5O_2 \leftrightarrow H_2O + 0.27O_2$$

$$H_2 + 0.77O_2 \leftrightarrow H_2O + 0.27O_2 \quad \rightarrow BALANCED$$

This indicates that for every mole of hydrogen burned, 0.77 moles of oxygen are needed not just the 0.5 moles required for stoichiometry because 0.27 moles are added to replenish the oxygen. To validate this, we compare the mass flow rate of oxygen (both burned and replenished) to that of hydrogen using their molar masses. The ratio must be greater than or equal to 0.77, as shown in Equation A.2:

$$((\dot{m}O_{2\ burnt} + \dot{m}O_{2\ replenish})/32) \div (\dot{m}H_{2\ burnt}/2) \geq 0.77 \qquad \text{(A.2)}$$

To compute the $\boldsymbol{\Phi}$ in the scramjet, we monitor how much oxygen is available compared to what is needed for stoichiometric combustion. The equivalence ratio is defined by Equation 2.4. To calculate the oxygen available from the freestream, we need the mass flow rate of the freestream air. In our vitiated air facility, the orifice size is too large for the choked flow assumption to hold. Instead, we use differential pressure measurements to calculate freestream mass flow rate, as shown in Equation A.3.

$$m = C_d \cdot A \sqrt{\left(\frac{2\rho(P_1 - P_2)}{1 - \left(\frac{d}{D}\right)^4} \right)} \qquad \text{(A.3)}$$

To verify this calculation, and since we lack a precise value for the discharge coefficient C_d, we also calculate the freestream mass flow rate using the choked mass flow equation at the nozzle exit (before the scramjet, given we now know our vitiated air composition using NASA

CEA) and apply mass conservation. By subtracting the known mass flow rates of the burnt and replenished O_2, H_2, and igniter fuels, the remainder should match the freestream mass flow rate determined using Equation A.3. This serves as a validation check. Once we confirm that the post-heater gas mixture contains 21% oxygen by mole, we calculate the equivalence ratio in the scramjet using Equation 2.4. In the scramjet itself, the stoichiometric reaction is simple:

$$H_2 + 0.5O_2 \leftrightarrow H_2O \quad \rightarrow BALANCED$$

Finally, for both the heater igniter and the scramjet igniter, we use **ethylene** (C_2H_4) as fuel. To ensure complete combustion, we target an $\boldsymbol{\Phi} = 1$ (stoichiometric), with the reaction:

$$C_2H_4 + 3O_2 \rightarrow 2CO_2 + 2H_2O \quad \rightarrow BALANCED$$

This ensures efficient combustion in all stages of the system while maintaining proper oxygen balance for accurate scramjet operation.

Appendix B

B.1 Hard Starting

Hard starting refers to an undesirable and potentially dangerous condition during the ignition phase of scramjet and rocket engines. It occurs when combustion begins in an over-pressurized environment, typically due to delayed ignition after significant accumulation of fuel and oxidizer in the combustion chamber. When ignition finally occurs, the rapid and uncontrolled combustion of the built-up propellants leads to a sudden pressure spike.

This abrupt rise in pressure often referred to as a pressure shock or overpressure event can result in:

- Structural damage to engine components, especially the combustor walls and injectors.
- Failure of seals and valves due to the rapid pressure loading.
- Complete engine failure, particularly in tightly confined or thin-walled combustion chambers.
- In extreme cases, vehicle loss, especially in experimental or high-performance systems.

In scramjet engines, which rely on supersonic airflow and careful flame holding, hard starts can destabilize the flow field, trigger inlet unstart, or destroy internal flame structures. In rocket engines, especially those using liquid propellants, hard starts often damage turbopumps or

combustion chambers due to the violent ignition pressure. Preventing hard starts involves careful control of ignition timing, propellant flow rates, and chamber pressure thresholds, as well as the use of pre-ignition purge cycles or staged ignition systems.

B.2 Avoiding Hard Start in the Vitiated Heater Facility

In our vitiated air heater facility, careful consideration has been given to avoid hard start conditions during the ignition phase. A hard start, characterized by a sudden and violent pressure spike due to delayed ignition of accumulated fuel and oxidizer, poses a serious risk to the structural integrity of the heater, downstream components, and overall test safety. To mitigate this, the system is specifically designed with a mechanical blowout port that functions as a pressure relief mechanism, as shown in Figure B.1.

Figure B.1: Picture of a ruptured blowout port

The blowout port is calibrated to release at 180 psia [13], serving as a critical safety feature. In the event of an abnormal pressure rise, which might occur during a delayed or failed ignition, the blowout port vents excess pressure to prevent catastrophic damage to the facility. This ensures that pressure within the combustion chamber is kept within structural limits, thereby protecting both the facility and personnel.

To further control and avoid hard starts, the following operational procedures and control strategies are implemented:

1. Sequenced Ignition and Fuel Flow Control: Fuel and oxidizer flow into the heater chamber is carefully sequenced so that ignition occurs before excessive mixing or buildup of reactants can take place (flame first before gases are introduced).

2. Purge Procedures Before Ignition: Prior to initiating a new ignition cycle, a pre-ignition purge with inert gas (such as nitrogen) is conducted to clear any residual fuel or hot gases from the chamber. This minimizes the risk of spontaneous or uncontrolled ignition from lingering fuel-air mixtures.
3. Real-Time Pressure Monitoring and Fast-Response Valve Closure: A safety officer monitors the pressure data of the system and listens for any malfunction in the heater section in real time. If an unexpected pressure rise is detected approaching the blowout threshold, the safety officer can call for a rapid shut-off fuel flow and abort ignition if necessary.

4. Reliable Igniter Performance: A high-energy, fast-response igniter is used to ensure consistent and immediate flame initiation, reducing the delay between fuel introduction and ignition.
5. Spark Plug Check: Given the igniters are running at stoichiometry, check spark plugs after 5 experiments and clean the deposited soot if present. The buildup of soot can cause a weak spark, leading to the failure of the igniter. Thus, causing a hard start.

By combining mechanical safeguards such as the 180 psi blowout port with procedural controls and real-time monitoring, the facility effectively mitigates the risk of hard starts. These measures are essential not only for protecting equipment but also for ensuring safe, repeatable, and high-fidelity experimental testing within the vitiated heater system. Below is an example of data collected during a hard start.

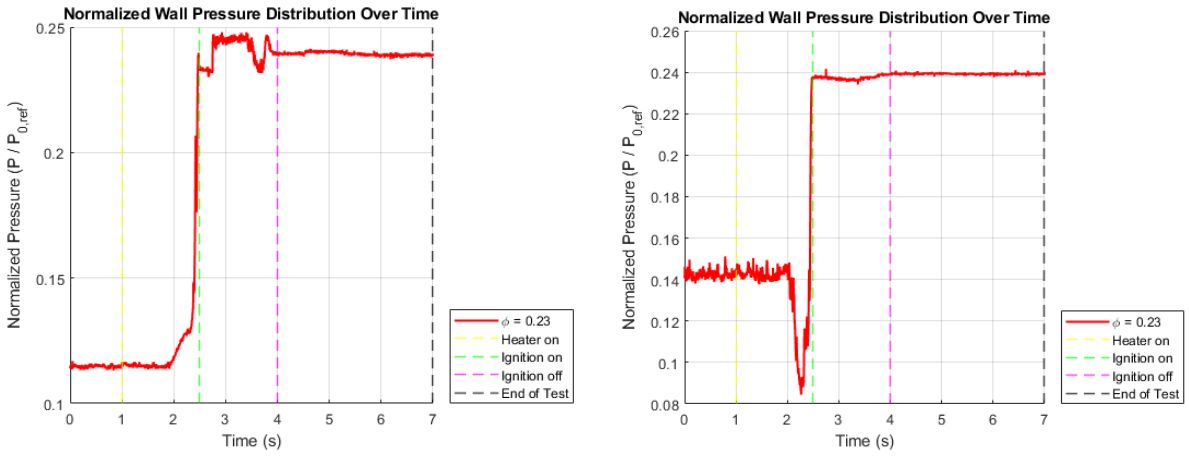

Figure B.2: Wall Pressure plot of the leading and trailing edge cavity port

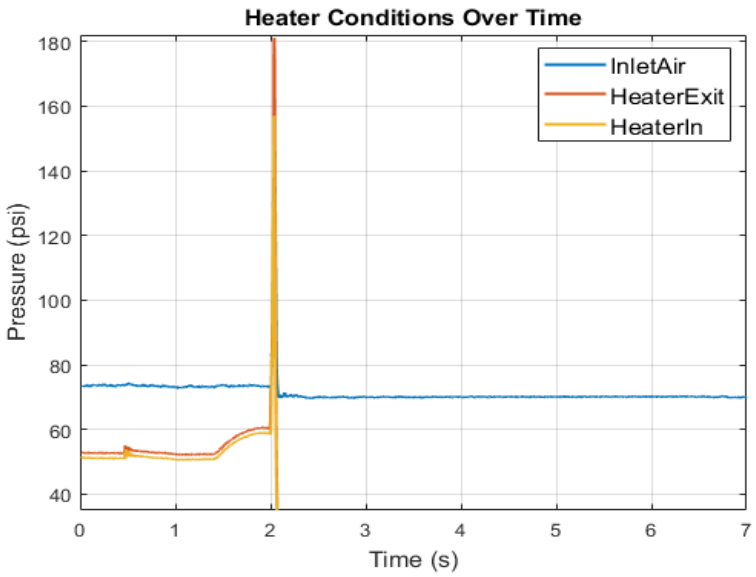

Figure B.3: Chamber pressure data during blowout

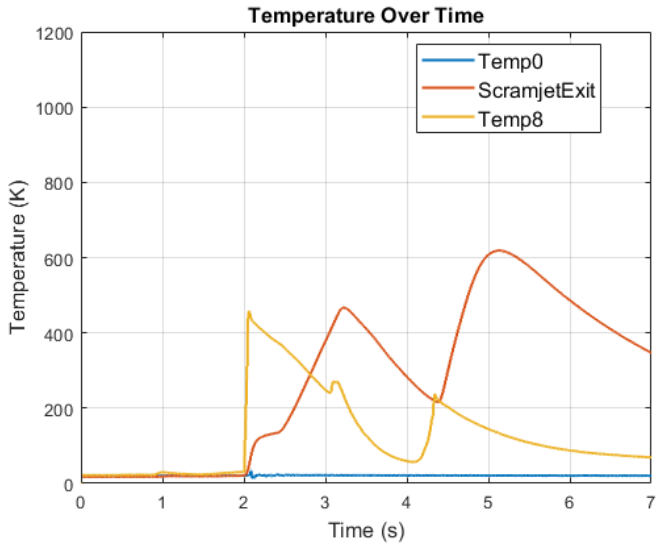

Figure B.4: Thermocouple temperature readings during blowout

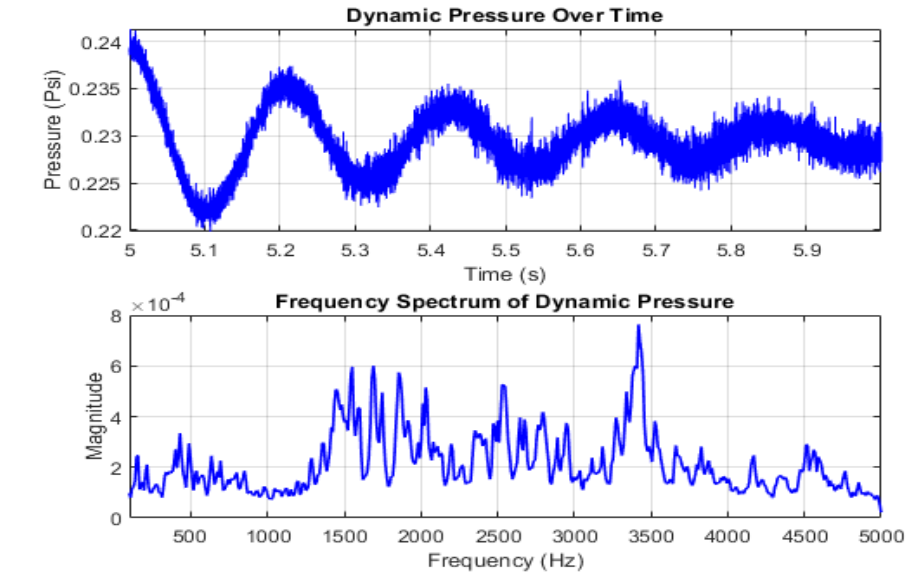

Figure B.5: Dynamic Pressure plot during blowout

Appendix C: Images from Camera Future Work Preliminary Result

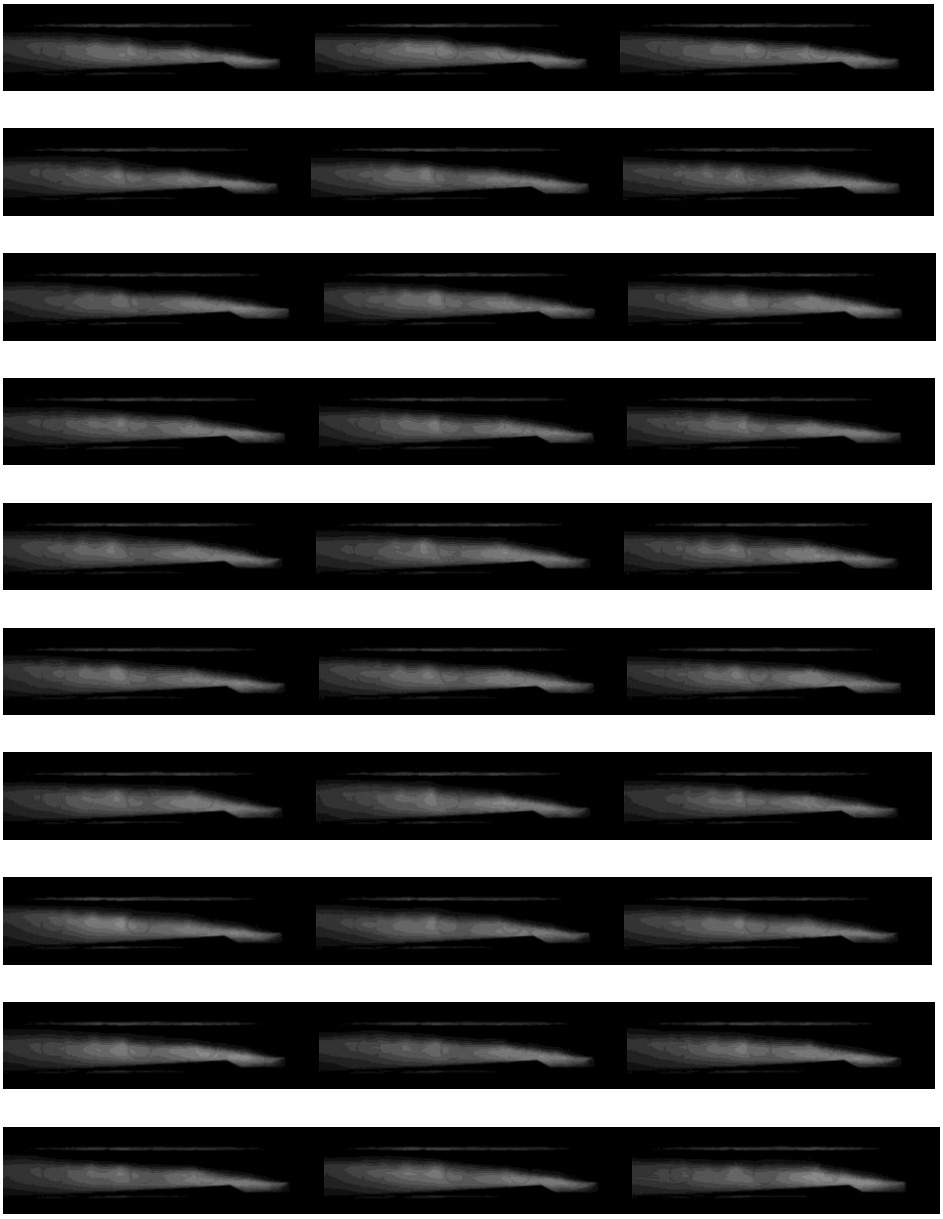

Figure C.1: High-speed camera sequence of the event 1ms apart for $\Phi = 0.23$

Figure C.2: High-speed camera sequence of the event 1ms apart for $\Phi = 0.24$

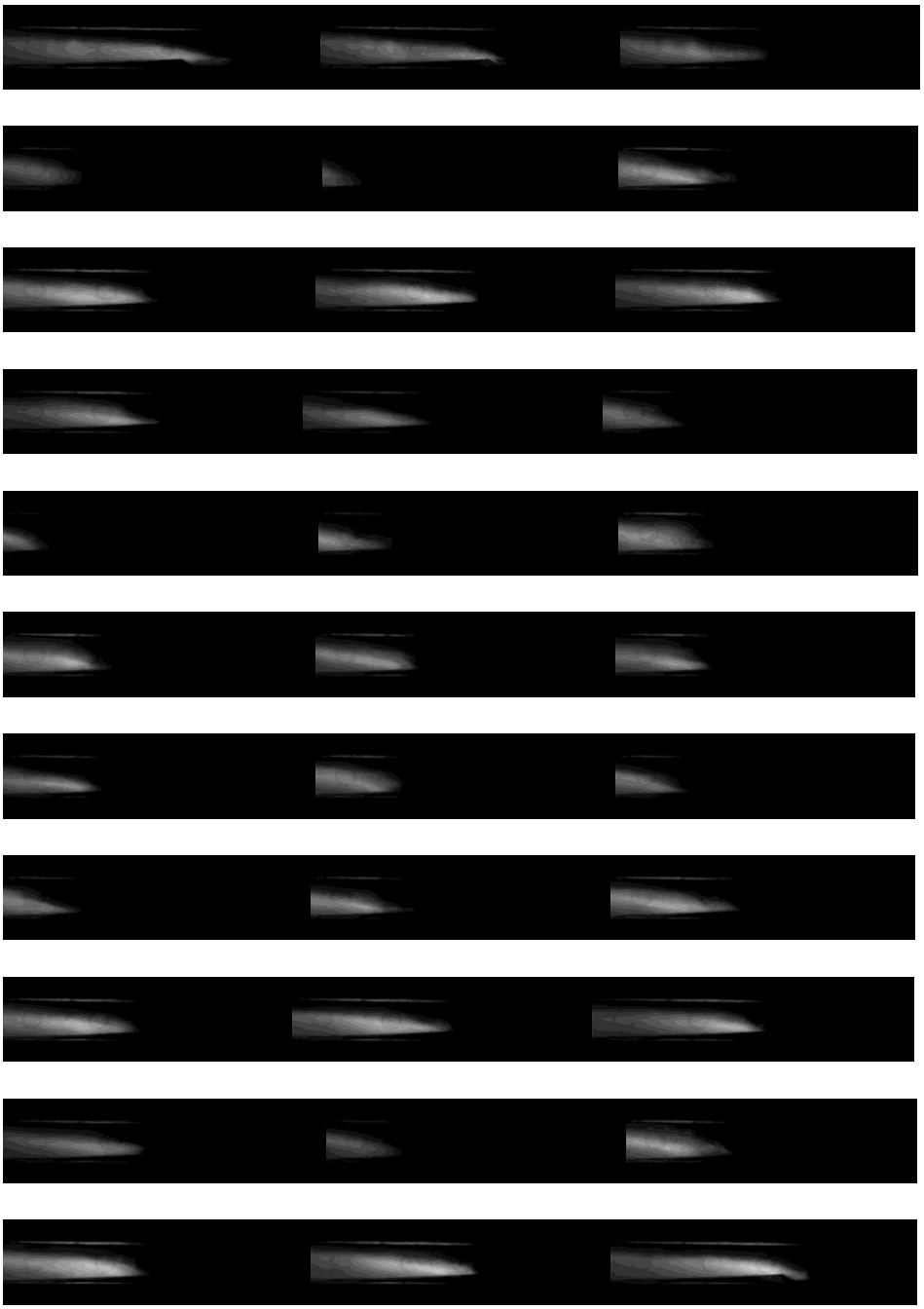

Figure C.3: High-speed camera sequence of the event 1ms apart for $\Phi = 0.25$

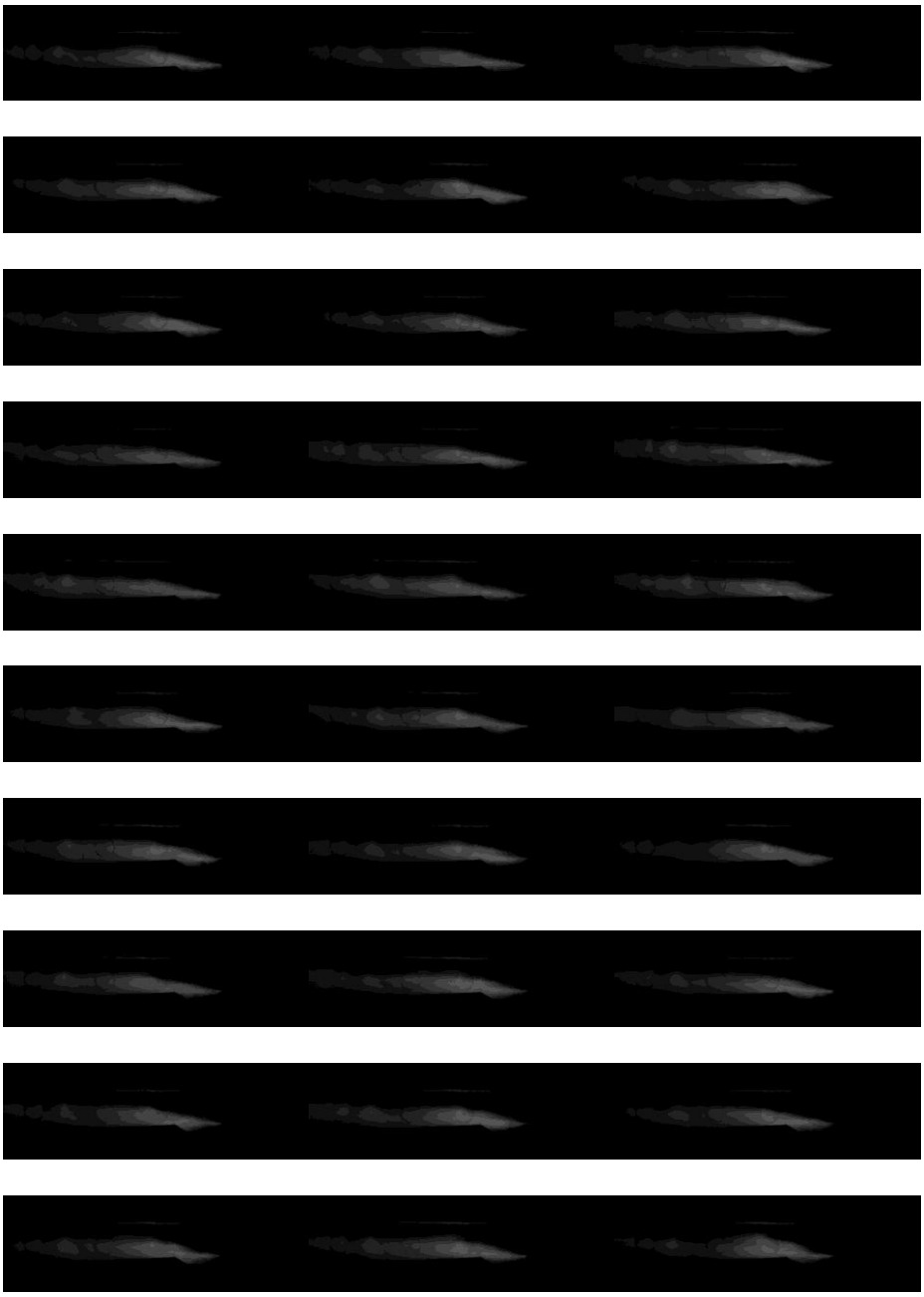

Figure C.4: High-speed camera sequence of the event 1ms apart for $\Phi = 0.26$

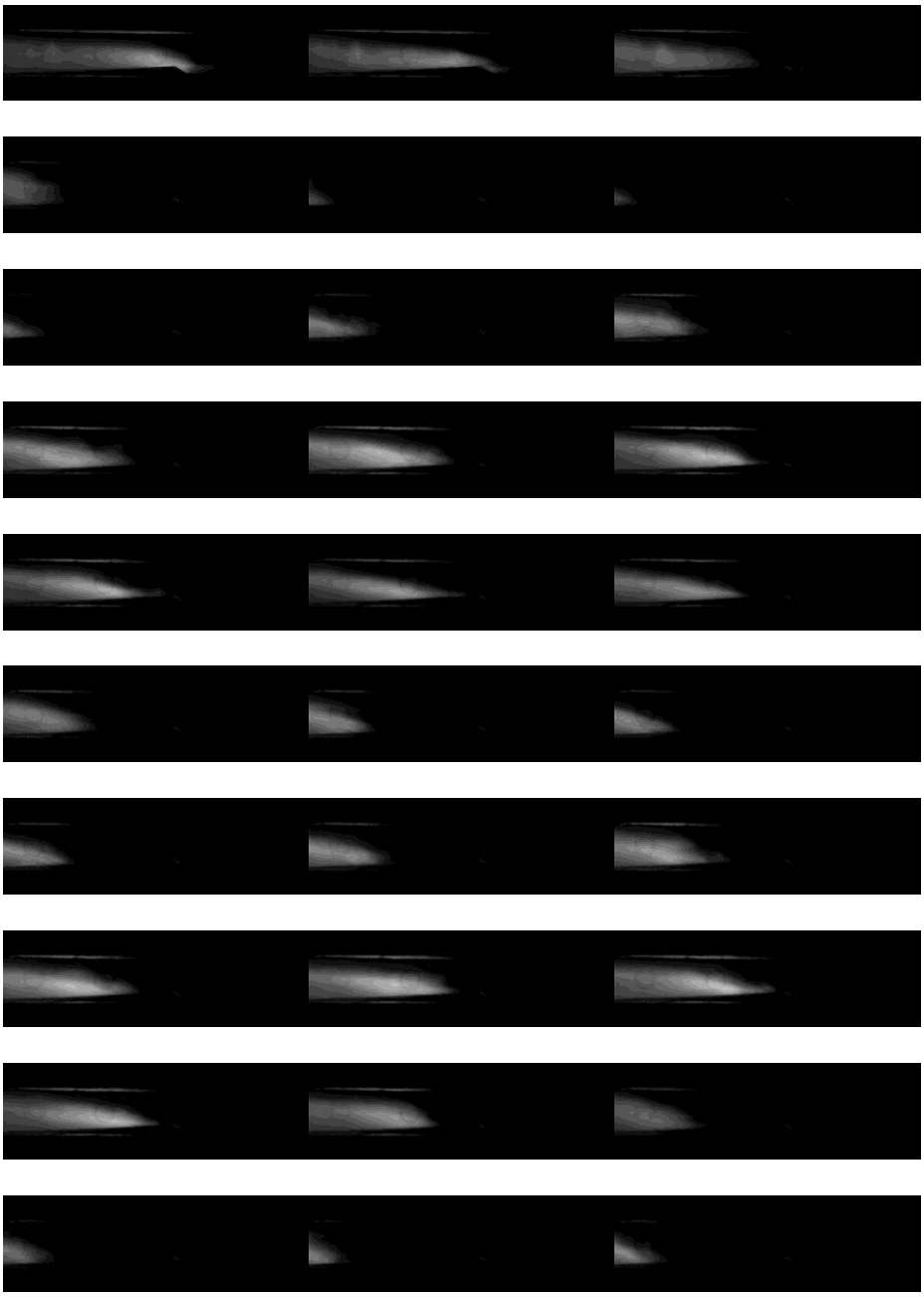

Figure C.5: High-speed camera sequence of the event 1ms apart for $\Phi = 0.3$

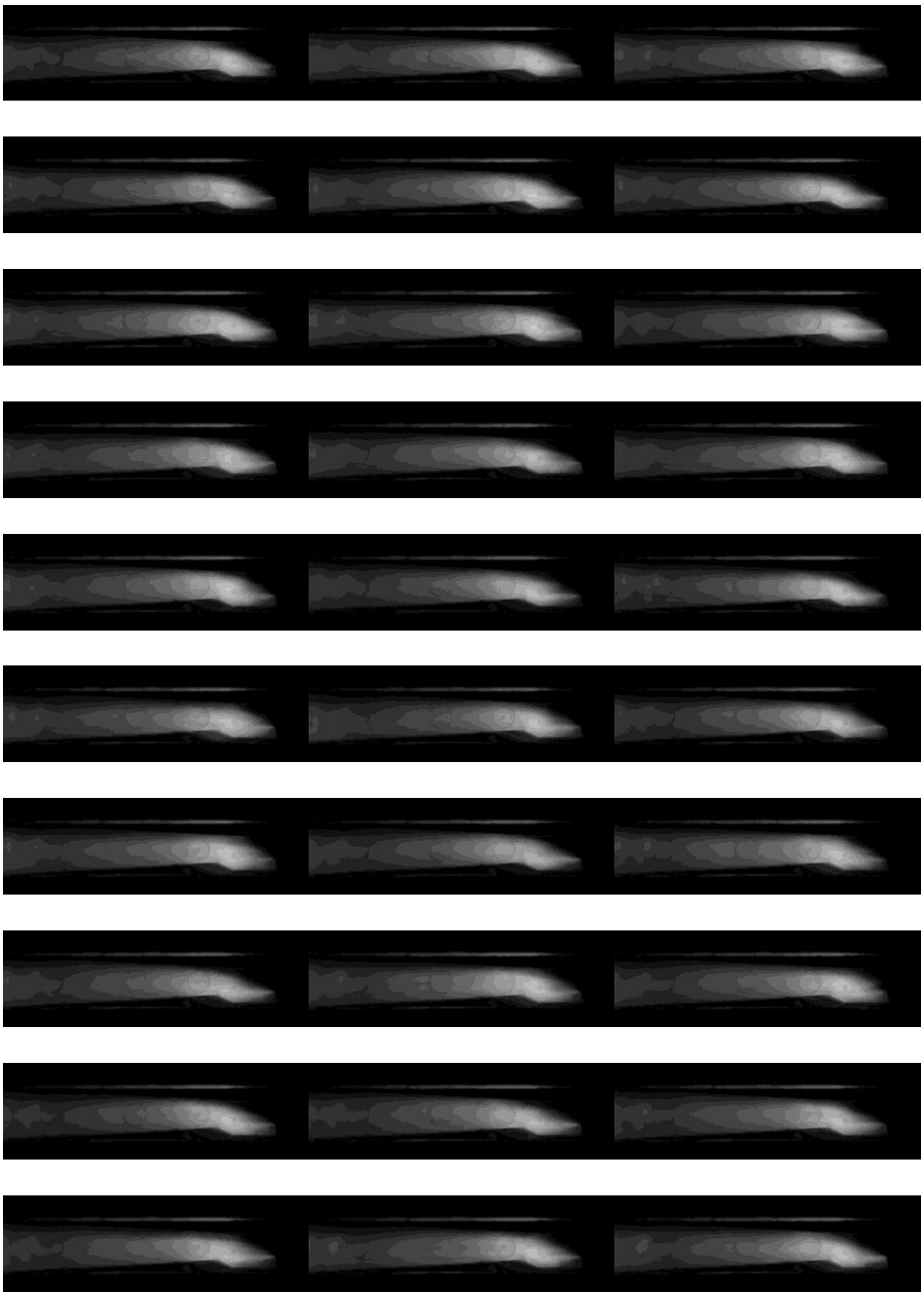

Figure C.6: High-speed camera sequence of the event 1ms apart for $\Phi = 0.43$

Appendix D: Dynamic Pressure Data

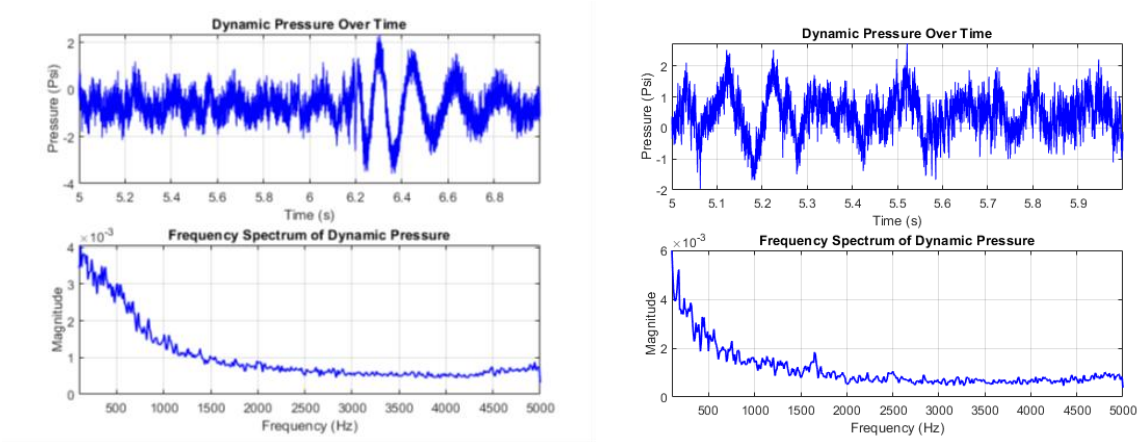

Figure D.1: Plot of Dynamic pressure vs time and FFT for Φ = 0.13(left) and 0.23(right)

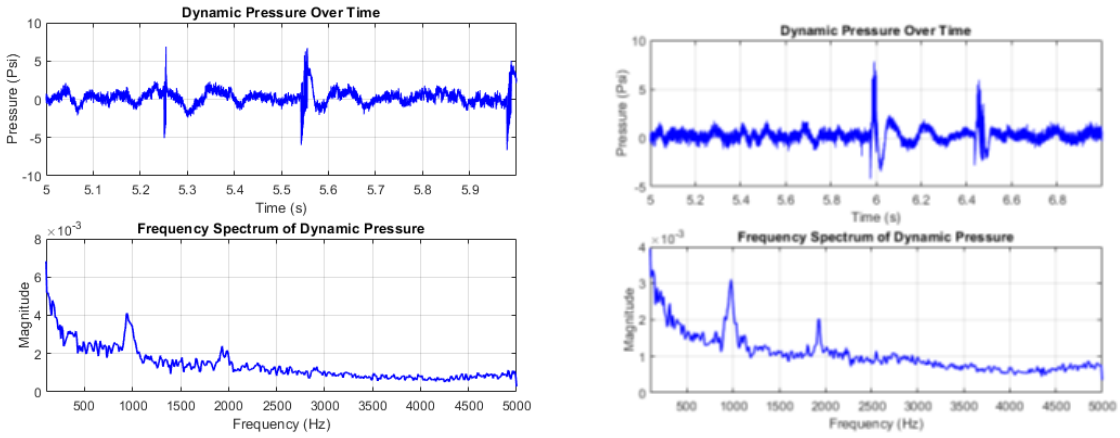

Figure D.2: Plot of Dynamic pressure vs time and FFT for Φ = 0.25(left) and 0.26(right)

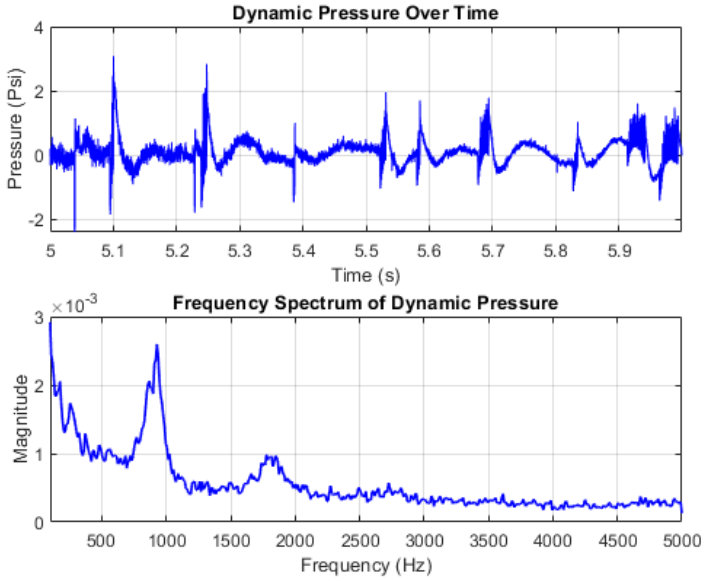

Figure D.3: Plot of Dynamic pressure vs time and FFT for $\Phi = 0.3$

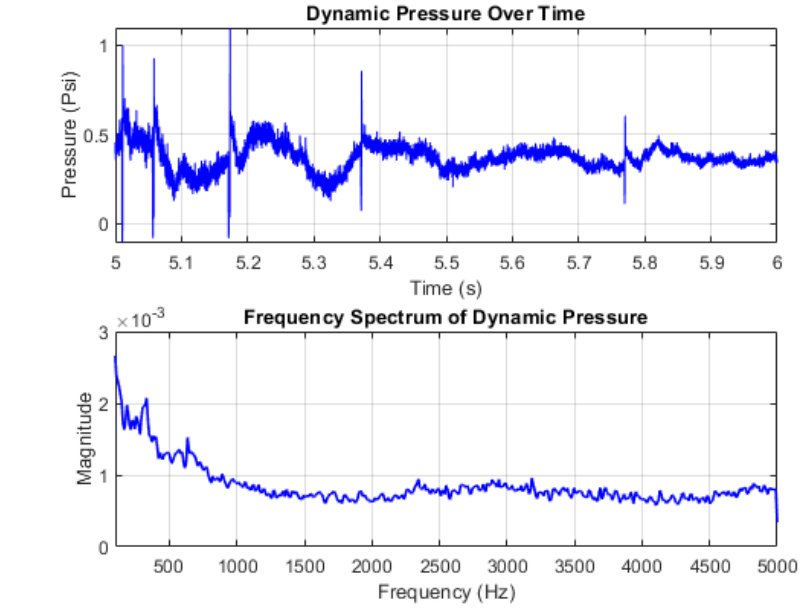

Figure D.4: Plot of Dynamic pressure vs time and FFT for $\Phi = 0.43$

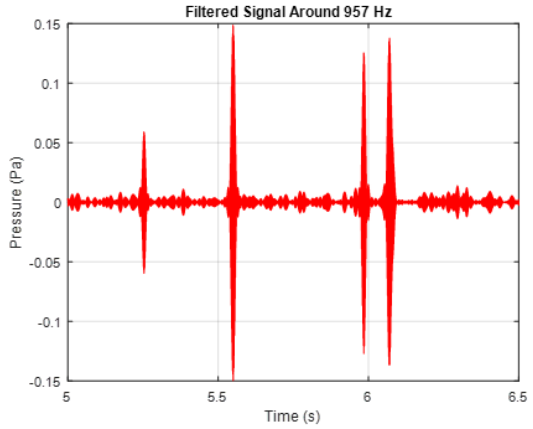

Figure D.5: Plot of dynamic pressure data of $\Phi = 0.25$ *through a high-pass filter*

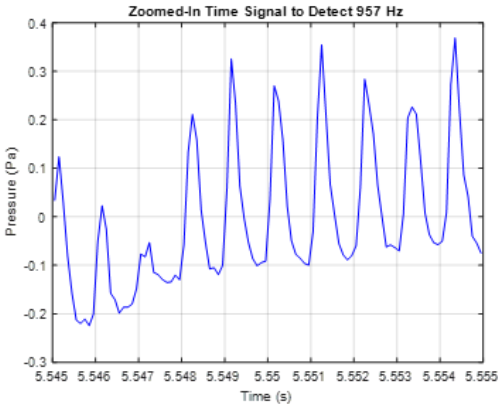

Figure D.6: Plot of dynamic pressure data of $\Phi = 0.25$ *to confirm presence of 957 Hz*

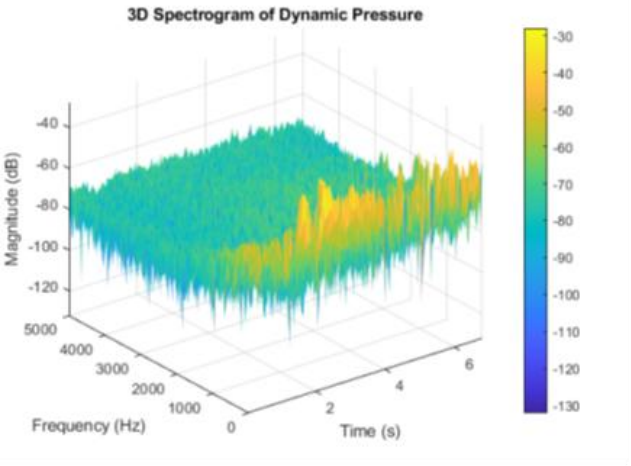

Figure D.7: 3D Plot of dynamic pressure data Spectrogram at $\Phi = 0.25$

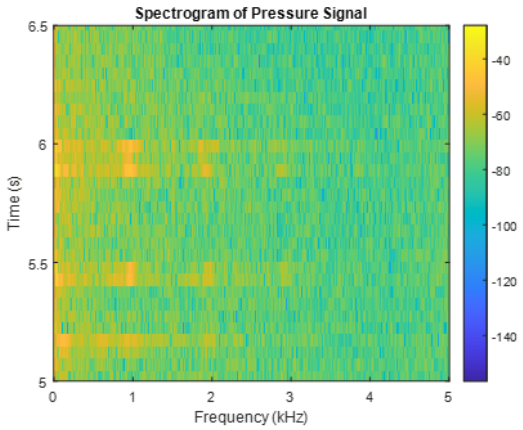

Figure D.8: 2D Plot of dynamic pressure spectrogram at $\Phi = 0.25$

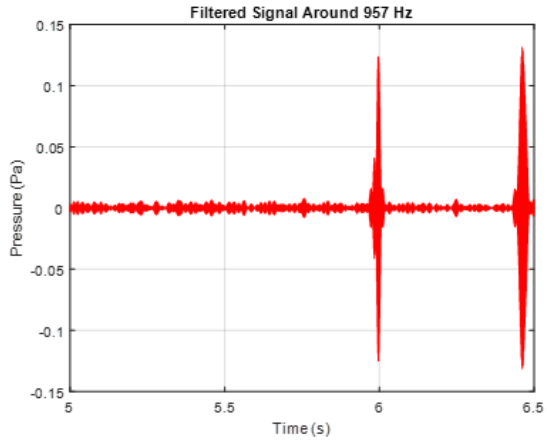

Figure D.9: Plot of dynamic pressure data of $\Phi = 0.26$ *through a high-pass filter*

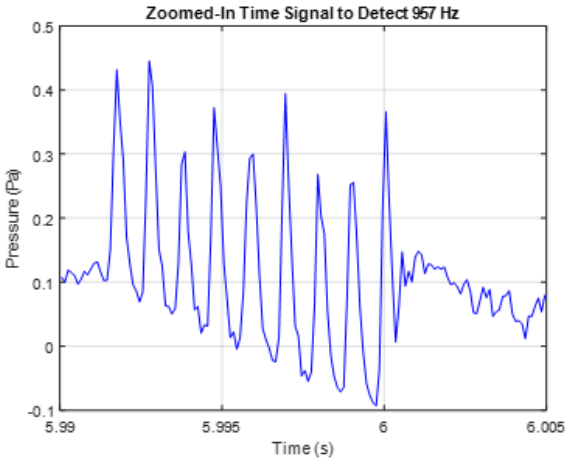

Figure D.10: Plot of dynamic pressure data of $\Phi = 0.26$ *to confirm presence of 957 Hz*

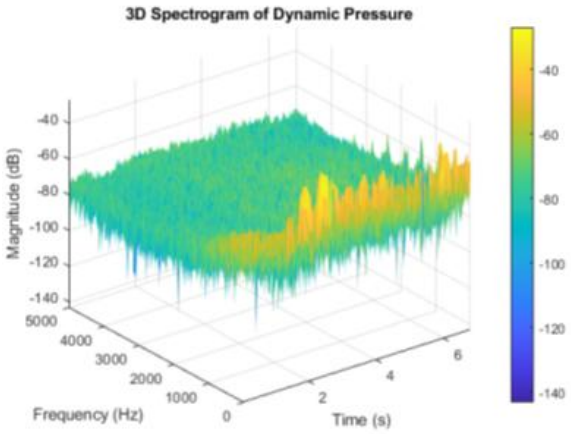

Figure D.11: 3D Plot of dynamic pressure data Spectrogram at $\Phi = 0.26$

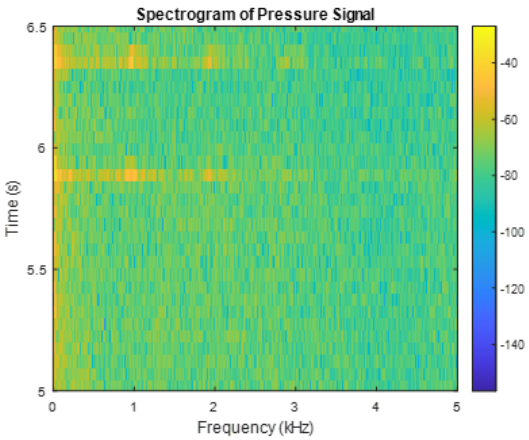

Figure D.12: 2D Plot of dynamic pressure spectrogram at $\Phi = 0.246$

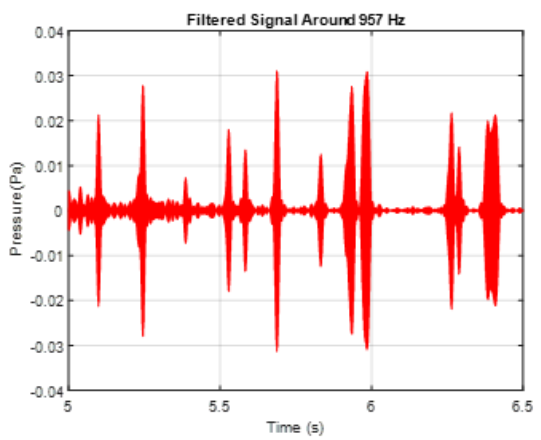

Figure D.13: Plot of dynamic pressure data of $\Phi = 0.3$ *through a high-pass filter*

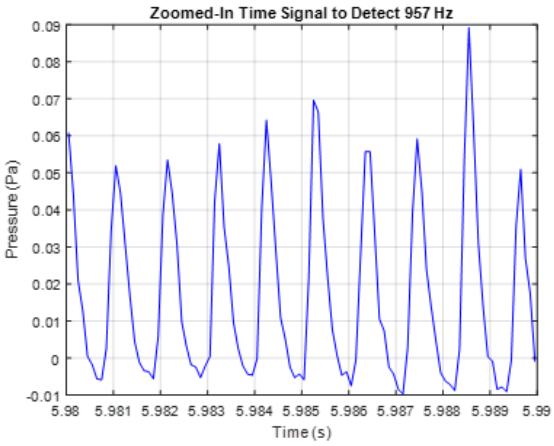

Figure D.14: Plot of dynamic pressure data of $\Phi = 0.3$ *to confirm presence of 957 Hz*

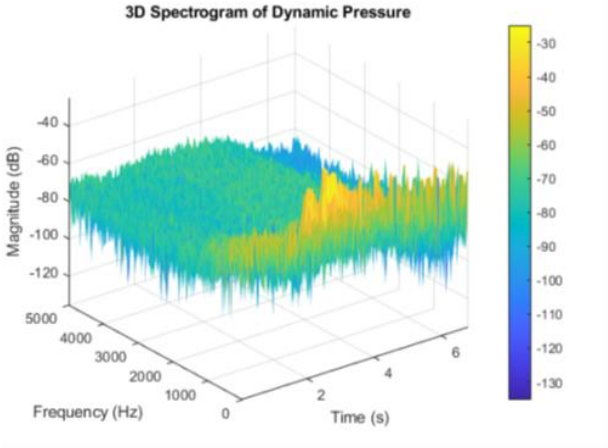

Figure D.15: 3D Plot of dynamic pressure data Spectrogram at $\Phi = 0.3$

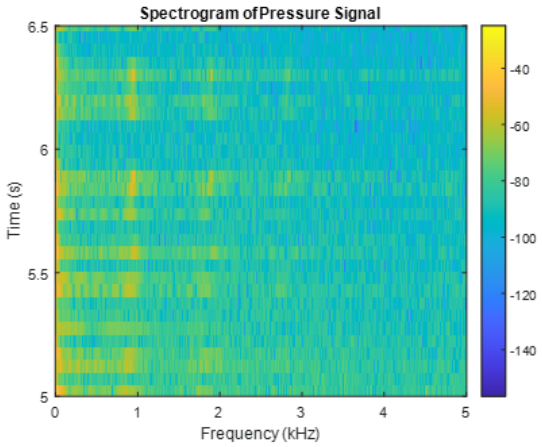

Figure D.16: 2D Plot of dynamic pressure spectrogram at $\Phi = 0.3$

Bibliography

[1] CNN, B. J. P. (2021, December 21). *Why a Mach 5 passenger plane is a crazy idea that might just work*. CNN. https://edition.cnn.com/travel/article/hypersonic-airplane-hermeus/index.html

[2] Waykul, M. (2023). Propulsion System in Hypersonic Spacecraft Rocket: A Review of Recent Development and Future Prospects. In *International Research Journal of Engineering and Technology*. https://www.irjet.net/archives/V10/i4/IRJET-V10I4230.pdf

[3] Staff, I. (2013a, May 9). *Knowledge Legacy – From the X-15 to the Space Shuttle | APPEL Knowledge Services*. Nasa.gov. https://appel.nasa.gov/critical-knowledge/case-studies/appel-case-studies/knowledge-legacy-from-the-x-15-to-the-space-shuttle/

[4] National Air and Space Museum. (2022b, July 7). *Speed and the Cold War*. Airandspace.si.edu. https://airandspace.si.edu/stories/editorial/speed-and-cold-war

[5] OptimizeIAS Team. (2022). https://optimizeias.com/air-breathing-scramjet-engine/

[6] *Air-Breathing Scramjet Engine - Optimize IAS*. (2022a, December 11). Optimize IAS. https://optimizeias.com/air-breathing-scramjet-engine/

[7] *Ramjet / Scramjet Thrust*. (2021). Nasa.gov. https://www.grc.nasa.gov/WWW/BGH/ramth.html

[8] Higham, E. (2022, June 13). *The Age of Hypersonic Weapons is Upon Us*. Microwavejournal.com; Microwave Journal. https://www.microwavejournal.com/articles/38245-the-age-of-hypersonic-weapons-is-upon-us

[9] Heiser, W. H., & Pratt, D. T. (1994). *Hypersonic airbreathing propulsion*. Washington, D.C American Institute Of Aeronautics And Astronautics.

[10] Sundermeier, S., Maximilian Passmann, Stefan, & Kenig, E. Y. (2022). Flow in Pillow-Plate Channels for High-Speed Turbomachinery Heat Exchangers. *International Journal of Turbomachinery Propulsion and Power*, *7*(2), 12–12. https://doi.org/10.3390/ijtpp7020012

[11] Jeong, S.-M., & Choi, J.-Y. (2020). Combined Diagnostic Analysis of Dynamic Combustion Characteristics in a Scramjet Engine. *Energies*, *13*(15), 4029. https://doi.org/10.3390/en13154029

[12] Kanapathipillai, M. (2022). *Scramjet combustor mode transition by controlling fuel injection distribution* [Doctoral dissertation, University of Maryland, College Park].

[13] Aguilera Muñoz, C. (2014). Effect of fin-guided fuel injection on supersonic mixing and combustion [Doctoral dissertation, Name of Institution]. ProQuest Dissertations & Theses Global.

[14] G.A. Sullins. Demonstration of mode transition in a scramjet combustor. J. Prop. Power, 9(4):515–520, 1993

[15] Meng, Y., Sun, W., Gu, H., Chen, F., & Zhou, R. (2022). Supersonic Combustion Mode Analysis of a Cavity Based Scramjet. *Aerospace*, *9*(12), 826. https://doi.org/10.3390/aerospace9120826

[16] O'Byrne, S., Doolan, M., Olsen, S. R., & Houwing, A. F. P. (2000). Analysis of transient thermal choking processes in a model scramjet engine. *Journal of Propulsion and Power, 16*(5), 808–814. https://doi.org/10.2514/2.5645

[17] Kim, C., Jeung, I., Choi, B., Matsubara, Y., Toshinori, Kouchi, & Masuya, G. (2009). A Study of Combustion Mode Transition using a New Supersonic Mixer in Dual-Mode Scramjet Engine.

[18] Curran, E. T., & Murthy, S. N. B. (2000). *Scramjet propulsion*. In *Progress in astronautics and aeronautics* (Vol. 189). AIAA.

[19] Gyu Sub Lee, & Lee, T. (2023). Fluid and combustion dynamics in dual-mode scramjets. *Frontiers in Aerospace Engineering*, *1*. https://doi.org/10.3389/fpace.2022.1058038

[20] Waltrup, P. J., & Billig, F. S. (1973). A study of the internal aerodynamics of hydrogen-fueled scramjet combustors. *Journal of Aircraft, 10*(11), 701-708.

[21] Zhao, G., Huang, Z., Zhang, L., & Sun, M. (2018). Effects of equivalence ratio on supersonic combustion in a scramjet combustor. *Aerospace Science and Technology*, *76*, 305-312.

[22] *General features*. (2015b, October 9). Aeronautics and Astronautics. https://www.aa.washington.edu/research/ramaccel/features

[23] Yu, K. H., Wilson, K. J., & Schadow, K. C. (2001). Effect of flame-holding cavities on supersonic combustion performance. *Journal of Propulsion and Power, 17*(6), 1369-1377. https://doi.org/10.2514/2.5877.

[24] Hall, N. (2015). *Schlieren Flow Visualization*. Nasa.gov. https://www.grc.nasa.gov/www/k-12/airplane/tunvschlrn.html

[25] Schmidt, B. (2015). *Schlieren visualization ae 104b*. https://shepherd.caltech.edu/T5/Ae104/Ae104b_handout2015.pdf

[26] NASA. (2019). *CEA-TEST*. Nasa.gov. https://cearun.grc.nasa.gov/

[27] MATLAB, Version R2023b, Natwick, Massachusetts: MathWorks, 2024.

[28] ANSYS Inc. (2023). *ANSYS [Computer software]*. https://www.ansys.com

[29] Leishman, J. G. (2023). Altitude Definitions & Measurement. *Eaglepubs.erau.edu*. https://doi.org/10.15394/eaglepub.2022.1066.n30

[30] Shock interaction induced heat flux augmentation in hypersonic flows [Scientific figure]. (2025). ResearchGate. https://www.researchgate.net/figure/Sketch-of-a-Laser-2-Focus-Velocimeter-L2F_fig4_356183915

[31] *The Composition of Earth's Atmosphere With Elevation*. (2014, August 1). MrReid.org. http://wordpress.mrreid.org/2014/08/01/the-composition-of-earths-atmosphere-with-elevation/

[32] Picone, J. M., Hedin, A. E., Drob, D. P., & Aikin, A. C. (2002). NRLMSISE-00 empirical model of the atmosphere: Statistical comparisons and scientific issues. *Journal of Geophysical Research: Space Physics*, *107*(A12), SIA 15-1-SIA 15-16. https://doi.org/10.1029/2002ja009430

[33] Emmert, J. T., Picone, J. M., Lean, J. L., & Knowles, S. H. (2004). Global change in the thermosphere: Compelling evidence of a secular decrease in density. *Journal of Geophysical Research: Space Physics*, *109*(A2). https://doi.org/10.1029/2003JA010176

[34] *Studypool Homework Help - Air breathing engines propulsion*. (2021). Studypool.com.

https://www.studypool.com/documents/6042266/air-breathing-engines-propulsion

[35] Wallace, J. M., & Hobbs, P. V. (2006). Atmospheric science: an introductory survey (Vol. 92). Elsevier.

[36] Anderson, J. D. (2021). *Fundamentals of aerodynamics*. McGraw-Hill Education